₁   fractalRegression: An R package for multiscale regression and fractal analyses

₂   Aaron D. Likens[1] & Travis J. Wiltshire[2]

₃   [1] Department of Biomechanics, University of Nebraska at Omaha

₄   [2] Department of Cognitive Science & Artificial Intelligence, Tilburg University

₅   Author Note

13   Abstract

14   Time series data from scientific fields as diverse as astrophysics, economics, human

15   movement science, and neuroscience all exhibit fractal properties. That is, these time series

16   often exhibit self-similarity and long-range correlations. This `fractalRegression` package

17   implements a number of univariate and bivariate time series tools appropriate for analyzing

18   noisy data exhibiting these properties. These methods, especially the bivariate tools

19   (Kristoufek, 2015a; Likens, Amazeen, West, & Gibbons, 2019a) have yet to be implemented

20   in an open source and complete package for the R Statistical Software environment. As

21   both practitioners and developers of these methods, we expect these tools will be of

22   interest to a wide audience of scientists who use R, especially those from fields such as the

23   human movement, cognitive, and other behavioral sciences. The algorithms have been

24   developed in C++ using the popular Rcpp (Eddelbuettel & Francois, 2011) and

25   RcppArmadillo (Eddelbuettel & Sanderson, 2014) packages. The result is a collection of

26   efficient functions that perform well even on long time series (e.g., $\geq 10{,}000$ data points).

27   In this work, we introduce the package, each of the functions, and give examples of their

28   use as well as issues to consider to correctly use these methods.

29   *Keywords:* long range correlation, fractal, multiscale, dynamical systems

30   Word count: 6,888

₃₁   fractalRegression: An R package for multiscale regression and fractal analyses

₃₂   **Introduction**

₃₃   Over time, many signals from living and complex systems exhibit systematic

₃₄ regularities and dependencies across spatial and temporal scales (Kello et al., 2010). These

₃₅ regularities often follow a power-law (i.e., self-similarity across scales) that are estimated

₃₆ using fractal analyses. Fractal analysis, in its many forms, has become an important

₃₇ framework in virtually every area of science, often serving as an indicator of system health

₃₈ (Goldberger et al., 2002), adaptability (Bak, Tang, & Wiesenfeld, 1987), control (Likens,

₃₉ Fine, Amazeen, & Amazeen, 2015), cognitive function (Euler, Wiltshire, Niermeyer, &

₄₀ Butner, 2016), and multi-scale interactions (Kelty-Stephen, 2017).

₄₁   In particular, various methods related to Detrended Fluctuation Analysis (DFA)

₄₂ (Peng et al., 1994) have rose to prominence due to their relative ease of understanding and

₄₃ broad applicability to stationary and non-stationary time series, alike. More specifically, in

₄₄ areas of the social and cognitive sciences, DFA, or variants of DFA, have been used to

₄₅ study, for example, reaction times (Van Orden, Holden, & Turvey, 2003), eye gaze

₄₆ (Stephen, Boncoddo, Magnuson, & Dixon, 2009), gait (Delignières & Torre, 2009;

₄₇ Hausdorff et al., 1996), limb movements (Delignières, Torre, & Lemoine, 2008), heart rate

₄₈ (Goldberger et al., 2002), and neurophysiological oscillations (Euler et al., 2016; Hardstone

₄₉ et al., 2012; Schaworonkow & Voytek, 2021). And, beyond an individual level, the methods

₅₀ have been used to study human-machine system interaction (Likens et al., 2015), tool use

₅₁ (Favela, 2020; Kelty-Stephen, Stirling, & Lipsitz, 2016), and interpersonal coordination in a

₅₂ variety of modalities (Davis, Brooks, & Dixon, 2016; Delignières, Almurad, Roume, &

₅₃ Marmelat, 2016).

₅₄   Thus, there is a broad scientific appeal for these fractal-based analyses. While, the

₅₅ basic DFA algorithm has been implemented in numerous packages and software programs,

₅₆ more advanced methods such as Multifractal Detrended Fluctuation Analysis (MFDFA)

(Kantelhardt et al., 2002), Detrended Cross Correlation Analysis (DCCA) (Podobnik & Stanley, 2008; Zebende, 2011), and, in particular, fractal regression techniques such as Multiscale Regression Analysis (MRA) (Kristoufek, 2015a; Likens et al., 2019a) have not yet been implemented in a comprehensive software package. A key aspect of this effort is to draw more attention and make more available these *fractal regression* techniques. In particular, we find these methods widely promising because they allow for uncovering "the time scales most relevant to relationships between a system's components" (p. 2) within a predictive framework (Likens et al., 2019a).

Thus, there is a clear need for a package that incorporates this functionality in order to advance theoretical research focused on understanding the time varying properties of natural phenomena and applied research that uses those insights in important and diverse areas such as healthcare (Cavanaugh, Kelty-Stephen, & Stergiou, 2017) and education (Snow, Likens, Allen, & McNamara, 2016). In this work, we provide an overview of our `fractalRegression` package, provide simulated and empirical examples of its functions, and provide practical advice on the successful application of these methods.

Package Overview

Our `fractalRegression` package for R (Team, 2018) is built on a C++ architecture and includes a variety of uni- and bivariate fractal methods as well as functions for simulating data with known fractional properties (e.g., scaling, dependence, etc.), and surrogate testing. Some foundational efforts in fractal analyses, which partially overlap with the functionality of this package, have been implemented elsewhere. For example, a number of univariate fractal and multifractal analyses have been implemented in the 'fracLab' library for MATLAB (Legrand & Véhel, 2003) and other toolboxes that are mainly targeted at multifractal analysis (Ihlen, 2012; Ihlen & Vereijken, 2010). In terms of open access packages, there are other packages that implement some, but not all of the same functions such as the `fathon` package (Bianchi, 2020) that has been implemented in

Python as well as the R packages: `fractal` [defunct], `nonlinearTseries` (Garcia, 2020), and `MFDFA` (Laib, Golay, Telesca, & Kanevski, 2018). However, none of the above packages incorporate univariate monofractal and multifractal DFA with bivariate DCCA and MRA and some are only written in base R code, which can be less efficient for long time series. Our `fractalRegression` package is unique in this combination of analyses and efficiency (particularly for long time series). For instance, we are not aware of any other packages that feature MRA. In addition, we expect that featuring simulation methods as well as surrogate testing strongly bolsters the accessibility of these methods for the social and cognitive science community in particular, but also science, more generally. An overview of the core functions included in the package, the general objective of that function, and the output are shown below in Table 1. Note that there are some additional helper and plotting functions included as well. The additional details are included in the sections corresponding to those methods, in the package documentation, and in the original sources for the methods.

Table 1.

Overview of core package functions, objectives, and output

Methodological Details and Examples

In order to demonstrate the methods within the `fractalRegression` package, we group this into univariate (DFA, MFDFA) and bivariate methods (DCCA, MRA). For each method, we 1) highlight the key question(s) that can be answered with that method, 2) briefly describe the algorithm with references to additional details (see also Appendix 1 for fundamental equations), 3) describe some key considerations for appropriately applying the algorithm, and demonstrate the use of the functions on a 4) simulated and 5) empirical example. Note that all code, data, and text are part of a reproducible manuscript that are accessible at the following link:

108 https://github.com/travisjwiltshire/fractal_regression_manuscript.

Univariate Methods

Detrended Fluctuation Analysis. A key question that can be answered by Detrended Fluctuation Analysis (DFA) (Peng et al., 1994) is: *what is the magnitude and direction of long range correlation in a single time series?* While DFA has been described extensively (Kantelhardt, Koscielny-Bunde, Rego, Havlin, & Bunde, 2001) and visualized nicely elsewhere (Kelty-Stephen et al., 2016), we provide a brief summary here. DFA entails splitting a time series into several small bins (e.g., 16). In each bin, a least squares regression is fit and subtracted within each window. Residuals are squared and averaged within each window. Then, the square root is taken of the average squared residual across all windows of a given size. This process repeats for larger window sizes, growing by, say a power of 2, up to $N/4$, where N is the length of the series. In a final step, the logarithm of those scaled root mean squared residuals (i.e., fluctuations) is regressed on the logarithm of window sizes. The slope of this line is termed α and it provides a measure of the long range correlation. α is commonly used an as estimator of the Hurst exponent (H), where $\alpha < 1$ = H, and for $\alpha > 1$, $H = 1 - \alpha$. Conventional interpretation of α is: $\alpha < 0.5$ is anti-correlated, $\alpha = 0.5$ is uncorrelated, white noise, $\alpha > 0.5$ is temporally correlated, $\alpha = 1$ is long-range correlated, 1/f-noise, pink noise, $\alpha > 1$ is non-stationary where the special case $\alpha = 1.5$ is fractional Brownian noise. More generally, $1 < \alpha < 2$ are referred to as fractional Brownian motion.

DFA Examples. To demonstrate the use of `dfa()` we simulate three time series using the `fgn_sim()` function. This is a simple function based on the former `fARMA` R package [defunct]. It requires the number of observations `n`, and the Hurst exponent `H`. In particular, we simulate white noise, pink noise, and anti-correlated fractional Gaussian noise using the code below.

```
white.noise <- fgn_sim(n = 5000, H = 0.5)


pink.noise <- fgn_sim(n = 5000, H = 0.9)


anti.corr.noise <- fgn_sim(n = 5000, H = 0.25)
```

133   Then, we run DFA on those simulated series using the example code below. Note

134 that this example uses linear detrending with minimum scale of 16, a maximum scale that

135 is at most 1/4 the time series length, and scale factor (`scale_ratio`) of 2, which is evenly

136 spaced in the logarithmic domain (see General Discussion for more details and

137 considerations for these parameter choices).

```
scales <- logscale(scale_min = 16, scale_max = 1024, scale_ratio = 2)


dfa.white <- dfa(x = white.noise, order = 1, verbose = 1,

scales=scales, scale_ratio = 2)


dfa.pink <- dfa(x = pink.noise, order = 1, verbose = 1,

scales = scales, scale_ratio = 2)


dfa.anti.corr <- dfa(x = anti.corr.noise, order = 1, verbose = 1,

scales = scales, scale_ratio = 2)
```
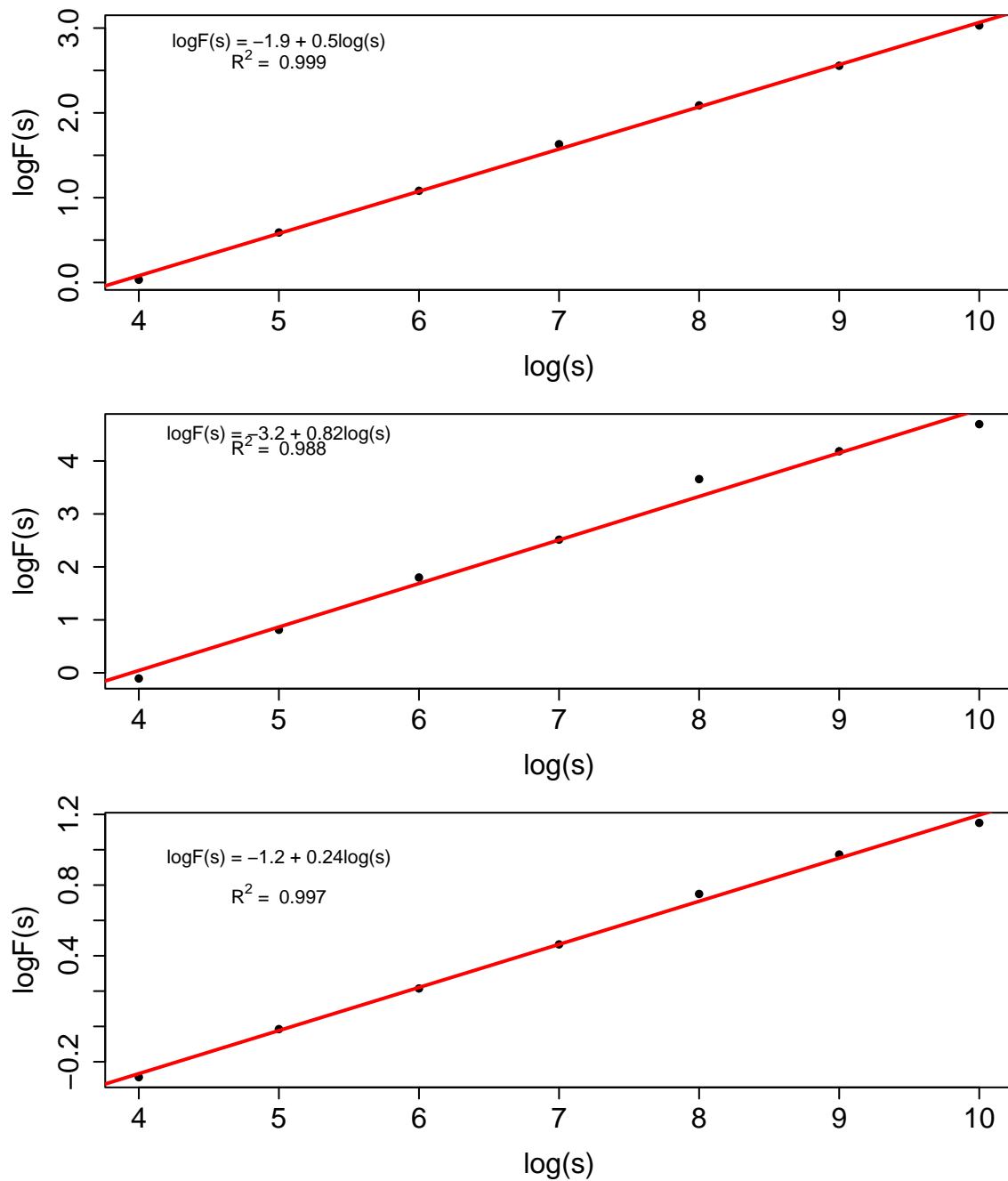
138   In terms of output from the above examples, for white noise, we observed that $\alpha =$

139 0.50, for pink noise we observed that $\alpha = 0.82$, and since we simulated anti-correlated noise

140 with $H = 0.25$, we observed a close estimate of $\alpha = 0.24$. In terms of the objects saved

141 from the `dfa()` function, one commonly inspects the log(scales)-log(fluctuation) plots,

142 which we generate from our package using the `dfa.plot()` function. Given the estimates

above, we see in Figure 1 that the slopes for white noise, pink noise, and anti-correlated

noise conform to our expectations. These slope estimates (and R^2) are provided in the

equation listed above each respective line.

Figure 1

Log scale-Log fluctuation plots for white noise (top), pink noise (middle), and

anti-correlated noise (bottom)

logF(s) = −1.9 + 0.5log(s)
R^2 = 0.999

logF(s) = −3.2 + 0.82log(s)
R^2 = 0.988

logF(s) = −1.2 + 0.24log(s)

R^2 = 0.997

149

For an empirical example, we apply the `dfa()` function to the Human Balance Dataset (Santos & Duarte, 2016). This publicly available dataset includes signals from a force platform that measures the center of pressure in the x and y dimensions for 87 young adults (we exclude the older adults from our analyses for simplicity). Trials lasted 60s. See original paper for additional details on data processing (Santos & Duarte, 2016). For the

155   empirical examples, we use two different time series featuring a participant standing on a

156   firm (rigid) surface with eyes open and a foam (unstable) surface with eyes open. We chose

157   this dataset because postural sway data are known to exhibit interesting fractal dynamics

158   (Collins & De Luca, 1993; Delignières, Torre, & Bernard, 2011a; Delignières, Torre, &

159   Bernard, 2011b) and we can systematically evaluate the data for all of the univariate and

160   bivariate analyses included in the package.

161   For center of pressure (COP) data, we take the first order differences of each series

162   using the `diff()` function as a rough approximation of COP velocity. For the univariate

163   analyses, we focus on analyses of the COP data in the x dimension. Then, we define the

164   appropriate scales for the analyses using the same methods shown above, except we use a

165   `scale ratio = 1.1` for a higher density of points. Figure 2 shows the results of these

166   analyses.

167   **Figure 2**

168   *Log scale-Log fluctuation plots for empirical differenced COPx time series for*

169   *rigid/firm (top) and unstable/foam (bottom) surfaces.*
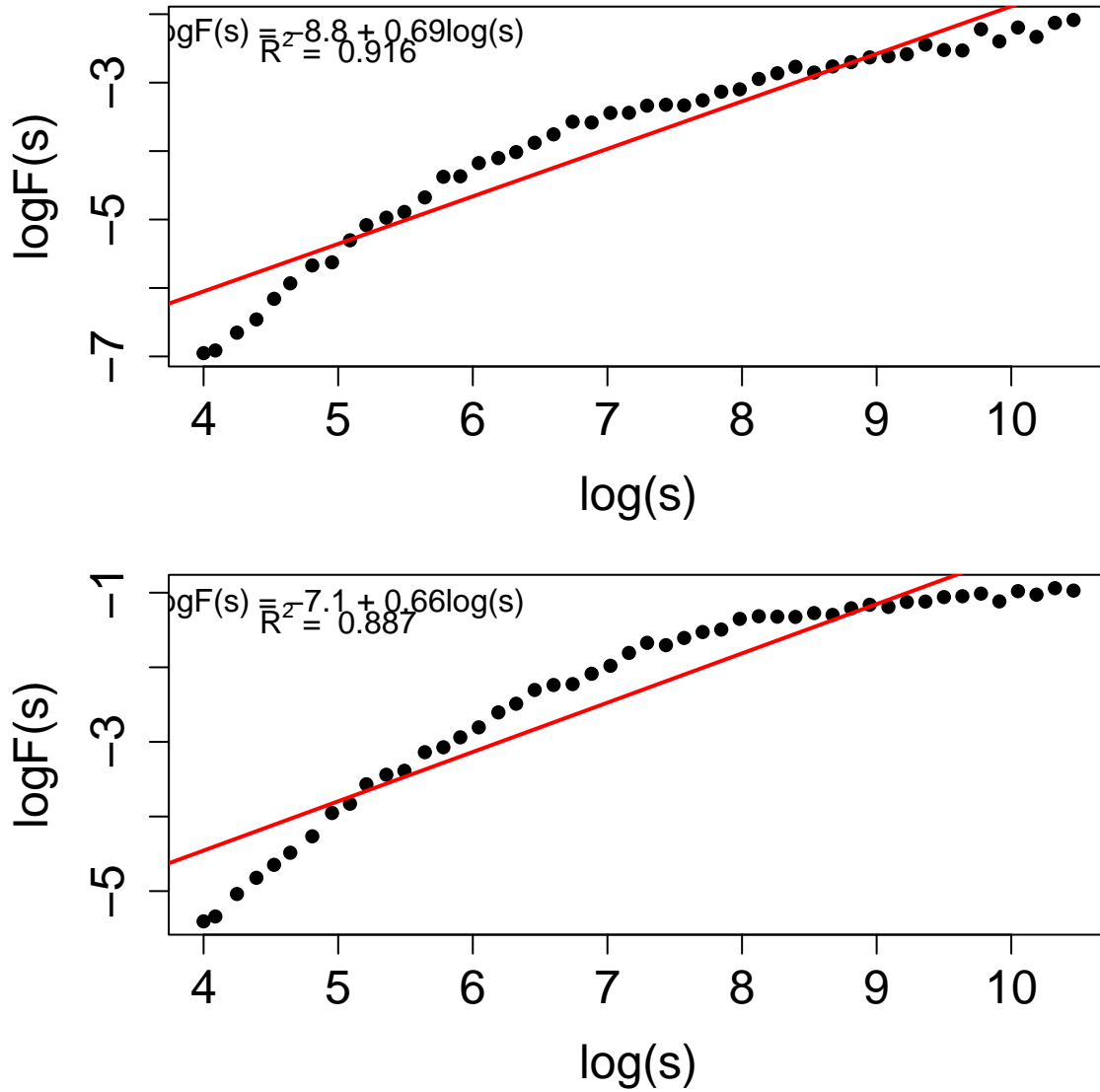
Importantly, regarding the question one can ask using DFA, we observe from Figure 2, that long range correlations are positive and approximately 0.69 - 0.66. However, from visual inspection of these plots we observe that two slopes might fit better than one for these time series; a phenomenon known as crossover points (Collins & De Luca, 1993; Ge & Leung, 2013). One common approach when such crossover points exist is to recognize that the signal might be best characterized by two scaling regions, before and after an inflection point. We provide an example of how to check for where the break point is below using piece-wise regression .

```
# requires the segmented R package


dfa.mod <- lm(log_rms ~ log_scales, data = open_firm_copx_diff_dfa)


seg <- segmented(dfa.mod, seg.Z = ~log_scales)
```
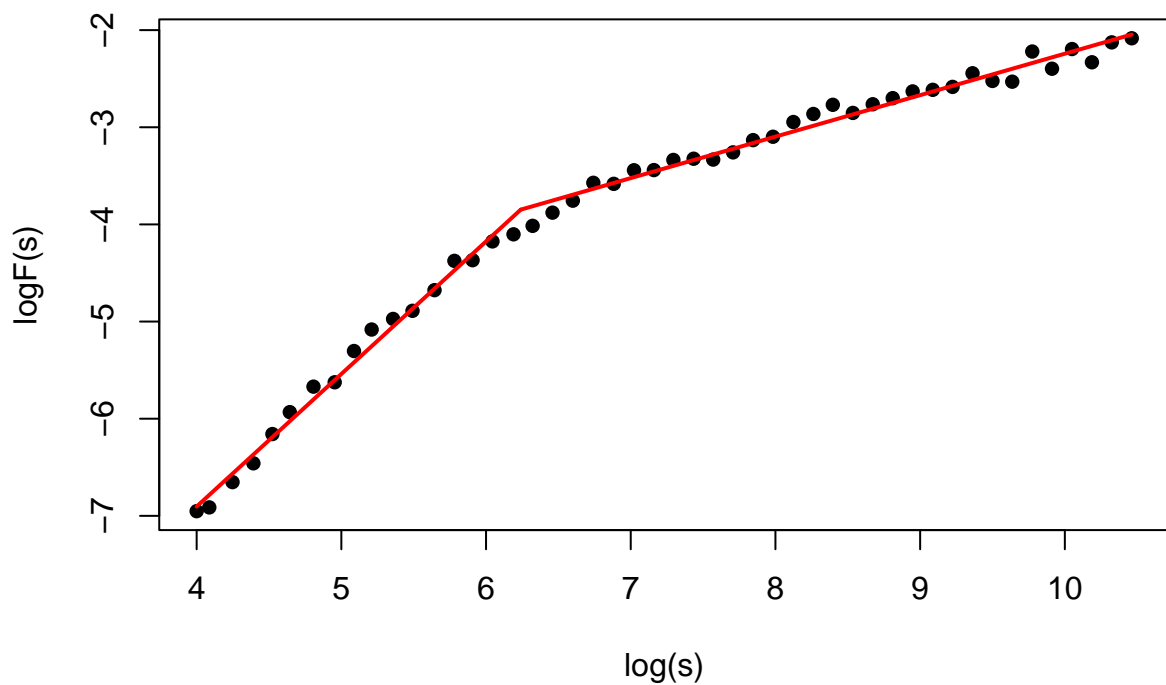
179   **Figure 3**

180   *Log scale-Log fluctuation plots for empirical differenced COPx time series for*

181   *rigid/firm surfaces with lines plotted for piece-wise regression slopes*

182

183   In the example above, we observe a crossover point at around the scale size of log 6.

184   And, from the results in Table 2 below, we observe that there are two distinct scaling

185   relationships corresponding to $\alpha = 1.36$ and $\alpha = 0.43$, respectively. This is a well known

186   result in the postural control literature such that short time scales exhibit a persistent

temporal correlation and that longer time scales exhibit an anti-persistent correlation. More substantively, short time scale dynamics correspond to periods of exploratory sway, whereas longer time scales correspond to corrective movements that prevent exceeding the base of support and falling (Collins & De Luca, 1993; Delignières et al., 2011a; Delignières et al., 2011b).

Table 2.

Results from piece-wise regression analysis

Multifractal Detrended Fluctuation Analysis. Multifractal Detrended Fluctuation Analysis (MFDFA; Kantelhardt et al. (2002)) is an extension of DFA by generalizing the fluctuation function to a range of exponents of the qth order. The key question that can be answered by MFDFA is: *how does the magnitude and direction of long range correlation change over time within a single time series?* Like DFA, MFDFA entails splitting a time series into several small bins (e.g., 16). In each bin, least squares regression is fit and subtracted within each window. However, the residuals are raised to a range of exponents q and averaged within each window. So when $q = 2$, MFDFA reduces to ordinary DFA. When $q > 2$, relatively larger residuals are emphasized and when $q < 2$, relatively smaller residuals are emphasized. The rest of the DFA algorithm is performed for each window and windows size for all values of q. We refer the reader to the work of Kelty-Stephens and colleagues' (Kelty-Stephen et al., 2016) Figure 3 for a visualization of the algorithm, Appendix 1 of this paper for fundemental equations, and Kantelhardt and colleagues' work (Kantelhardt et al., 2002) for additional mathematical description.

MFDFA Examples. To demonstrate the use of `mfdfa()`, we work with data included in our package (`fractaldata`), that was originally provided by Ihlen (2012). It includes a white noise time series, a monofractal time series, and a multifractal time series. These data are shown below in Figure 4.

Figure 4

213   *Time series from Ihlen (2012) corresponding to white noise, monofractal, and*

214 *multifractal series*

White Noise

Monofractal

Multifractal
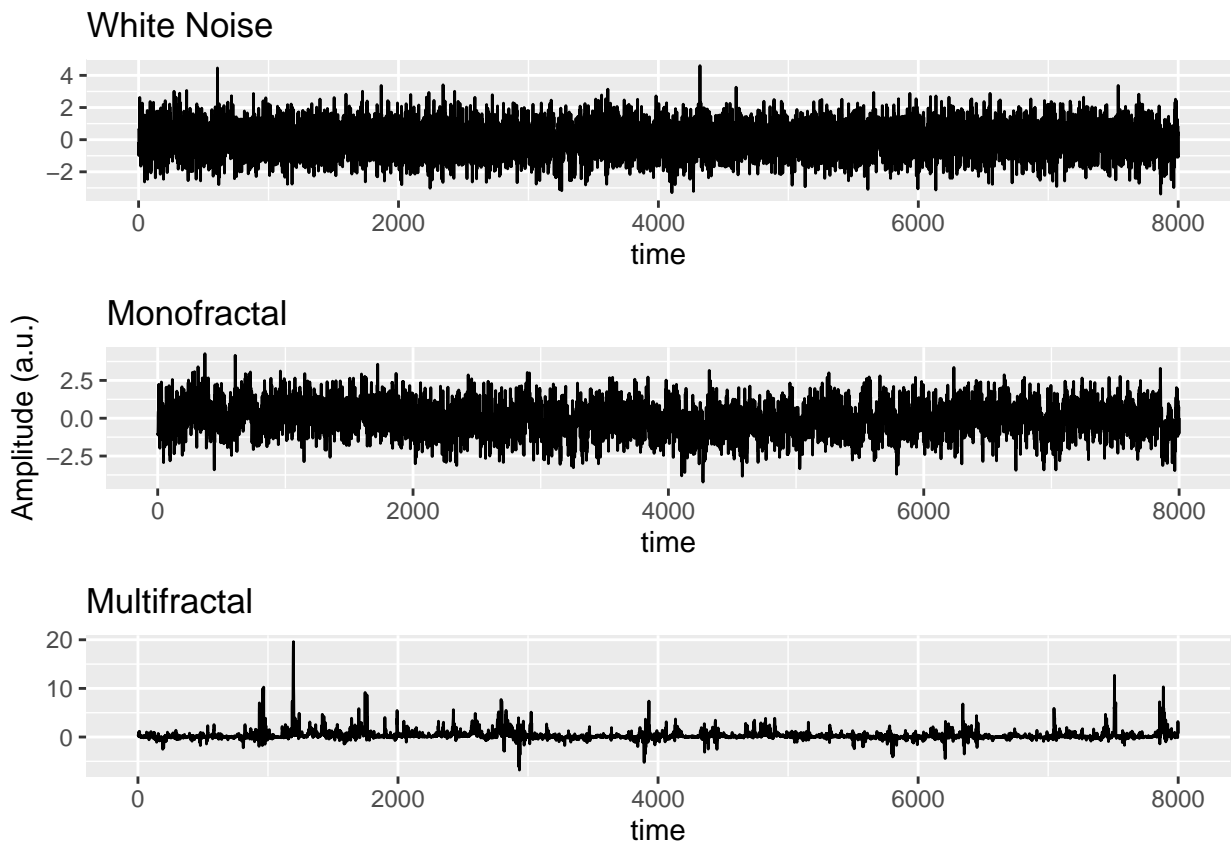
215

216   Performing MFDFA is straight forward with the `mfdfa()` function. As shown in the

217 example below, one enters the time series `x` to perform the analysis on, the range of `q` order

218 exponents to use, the `order` of polynomial detrending, and the `scales` for the analysis. In

219 this case, we define our `scales` by choosing logarithmically spaced scales and we select

220 values of q from -5 to 5. Note here that the scale factor need not be a power of two but

221 should be evenly spaced in the logarithmic domain by, for example, using different

222 logarithm bases. We provide the `logscale()` function to facilitate scale construction.

```
scales <- logscale(scale_min = 16,scale_max = 1024,scale_ratio = 1.1)


white.mf.dfa.out <- mfdfa(x = fractaldata$whitenoise, q = c(-5:5),
```

```
order = 1, scales=scales, scale_ratio=1.1)


mono.mf.dfa.out <- mfdfa(x = fractaldata$monofractal, q = c(-5:5),

order = 1,  scales=scales, scale_ratio=1.1)



multi.mf.dfa.out <- mfdfa(x = fractaldata$multifractal, q = c(-5:5),

order = 1,  scales=scales, scale_ratio=1.1)
```

₂₂₃   A common way to understand if there is evidence of multifractality is to examine a

₂₂₄ plot showing the slopes of the `log_fq` at the `log_scale` values. If all the lines have the

₂₂₅ same slope, that provides evidence of monofractality. If there are distinct slopes, then there

₂₂₆ is evidence of multifractality. It's also important to check here that the slopes of

₂₂₇ `log_scale` and `log_fq` are approximately linear, thus implying that they are scale

₂₂₈ invariant. If not, then it could be the case that a higher order polynomial detrending is

₂₂₉ appropriate (see Kantelhardt et al., 2001). Figure 5, in the top left quadrants, shows what

₂₃₀ we would expect for a monofractal and multifractal signal. In other words, the monofractal

₂₃₁ signal shows a consistent slope, whereas the multifractal signal shows variability in the

₂₃₂ slopes. Importantly, Figure 5, using our `mfdfa.plot()` function, shows various aspects of

₂₃₃ mfdfa for each value of q (each with its own color) and includes panels that show the

₂₃₄ log(scale)-log(Fluctuation) plots like in the DFA plots (top left), the slopes of those lines as

₂₃₅ the q-order Hurst exponents $H(q)$ for each value of q (top right), the mass exponents

₂₃₆ $(\tau(q))$ for each value of q (bottom left), and the multifractal spectrum showing q-order

₂₃₇ singularity values (h) for their dimension (D(h) for each value of q (bottom right). See

₂₃₈ Ihlen (2012) for additional details of these metrics.

₂₃₉   **Figure 5**

₂₄₀   *Mfdfa.plots for mono-(top) and multifractal series (bottom)*
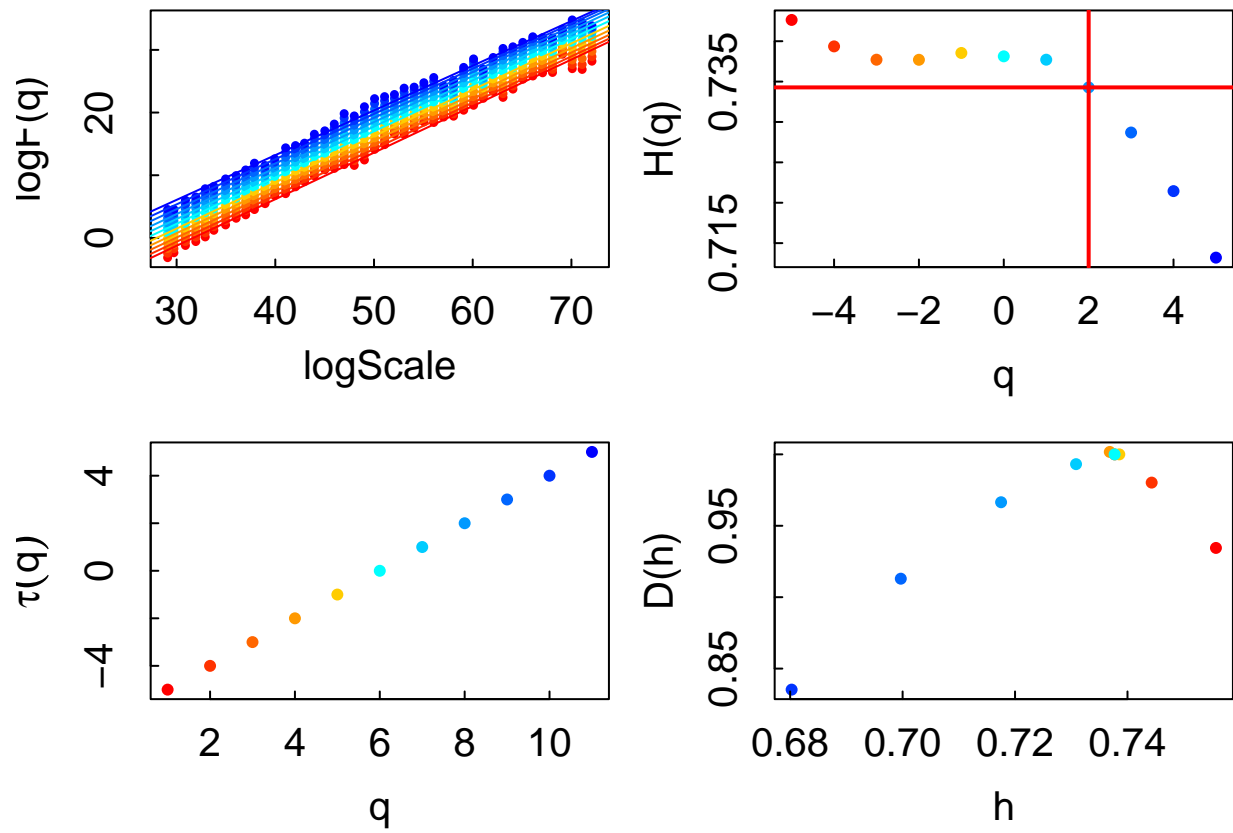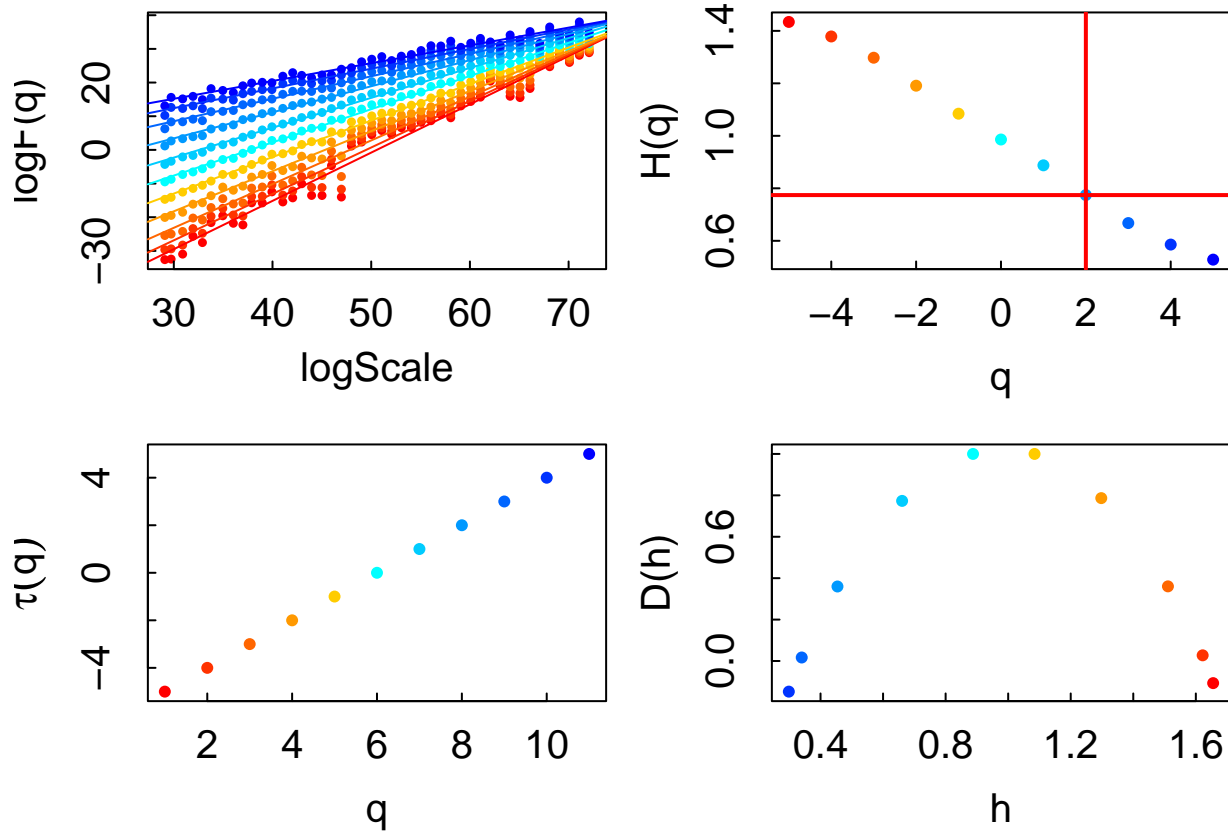
A common metric for comparing multifractal spectra is to calculate the width (W) as $h_{max} - h_{min}$. Let's do this to compare the monofractal and multifractal time series. We observe in this case that for the monofractal signal $W_{mono} = 0.08$ and $W_{multi} = 1.36$. If we compare the spectra for the mono- and multifractal signals above (bottom right of both plots), we observe this clear difference in the widths of the multifractal spectra for the signals.

For our empirical analysis, we again turn to the postural data. We set our parameters appropriate for the data and run `mfdfa()` on the differenced COPx data for the firm and foam surfaces. Figure 6 shows the plots for these analyses. In particular, we observe for both surfaces that the q-order Hurst exponents range from 0.57 - 1.03, all suggesting positive long-range correlations with a weakening of the strength at larger values of q (i.e., trending towards white noise). The multifractal spectrum widths of the two surfaces were also similar, $W_{foam} = 0.69$ and $W_{firm} = 0.70$.

256   **Figure 6**

257   *Mfdfa.plots for the firm (top) and foam surfaces (bottom)*

258

259
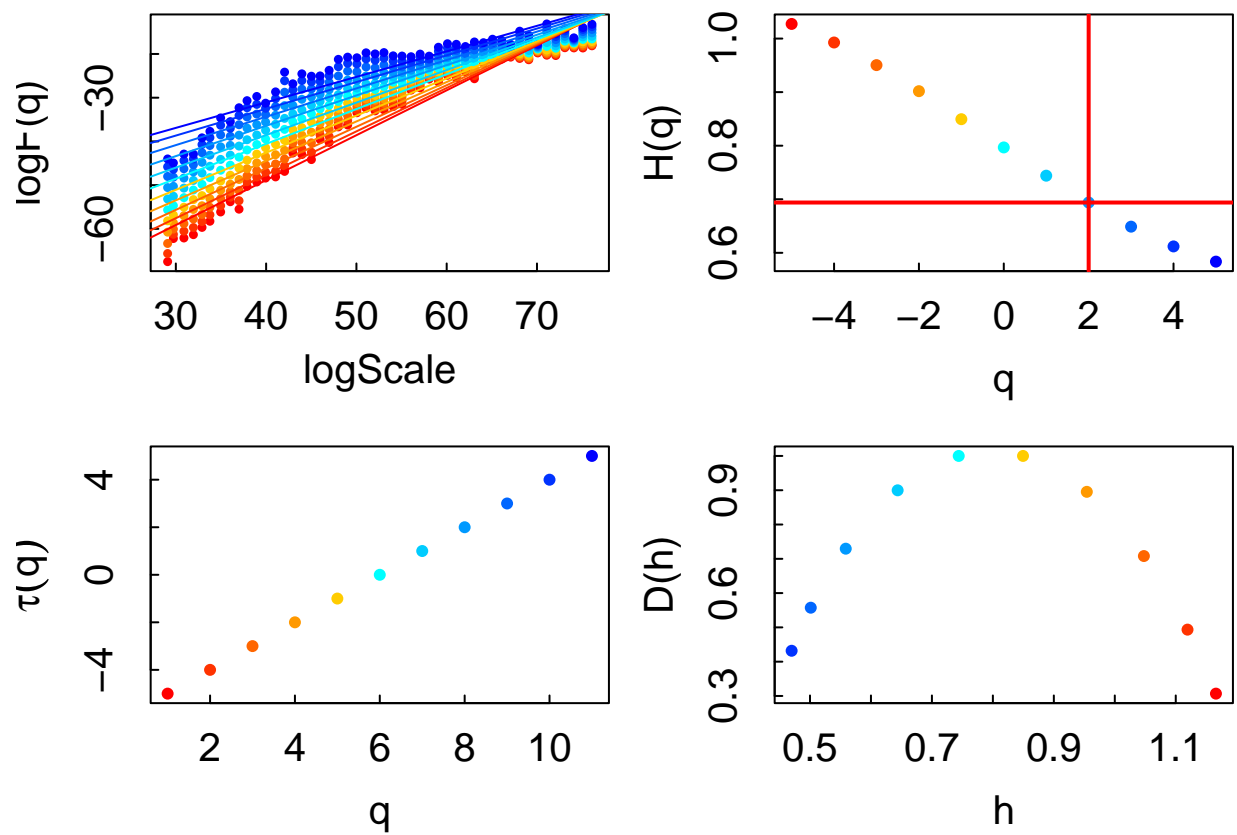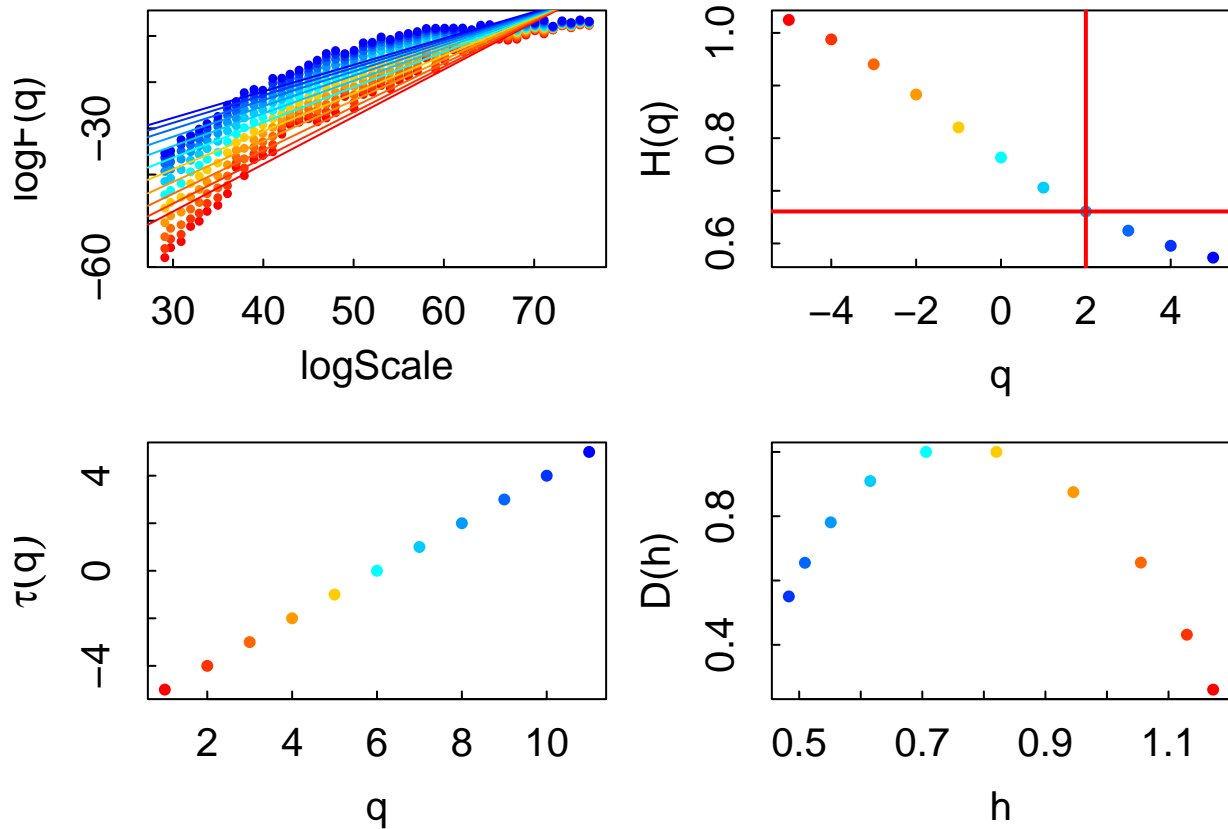
Bivariate Methods

Detrended Cross-Correlation Analysis. Detrended Cross-Correlation Analysis (DCCA (Podobnik & Stanley, 2008; Zebende, 2011) is a bivariate extension of the DFA algorithm generalizing it to a correlational case between two time series that may be non-stationary. The key questions that can be asked with it are: a) *How does the correlation between two time series change as a function of scale?* and b) *What is/are the dominant (time) scale(s) of coordination?* Such decisions are based on a predetermined threshold such as a conventional statistical significance as we demonstrate below. Researchers may also select other criteria appropriate for their research area.The DCCA algorithm is a direct generalization of the DFA algorithm but applied to two concomitantly measured time series, say x and y. As in DFA, time series are split into multiple bins and detrended using least squares regression. Separate regressions are performed for x and y.

272 Within each bin, three quantities are estimated, the average squared residual of x, the

273 average squared residual of y, and the average cross product (i.e., the covariance) between

274 the residuals for x and the residuals for y. Each of those quantities is averaged across all

275 bins of a given size. After taking the squared residual for x and y, we obtain scale-wise

276 equivalents of covariance $F_{xy}(s)$ and standard deviations for x $F_x(s)$ and y $F_y(s)$. The use

277 of F to designate these quantities derives from originating literature (Kristoufek, 2015b;

278 Likens, Amazeen, West, & Gibbons, 2019b). Thus, the scale-wise regression coefficient, the

279 estimand of DCCA, is the following quotient:

$$\rho(s) = \frac{F_{xy}(s)}{F_x(s)F_y(s)}$$

280   Simplified, like DFA, the key metric is α, but in DCCA, one estimates the

281 scale-specific, detrended cross-correlation coefficient $\rho(s)$ for the pair of time series.

282   ***DCCA Examples.*** To demonstrate the use of `dcca()`, we used the `mc_arfima()`

283 function from our package to simulate two time series with known properties. Specifically,

284 we use the multicorrelated ARFIMA examples from Kristoufek's work (Kristoufek, 2013).

285 In this case, we use the parameters from Kristoufek (2013) for Model 1 (p. 6,487), that

286 generates two time series of length 10,000 that exhibit long range correlations (LRC) as well

287 as long range cross-correlations (LRCC). The code for simulating these two time series is

288 shown below. Additionally, Figure 7, shown below, visualizes a subset of these time series.

```
set.seed(987345757)


sim1 <- mc_ARFIMA(process="Mixed_ARFIMA_ARFIMA", alpha = 0.2,

beta = 1, gamma = 1, delta = 0.2, n = 10000, d1 = 0.4, d2 = 0.3,

d3 = 0.3, d4=0.4, rho=0.9)
```

289   **Figure 7**

290   *Subset of two time series exhibiting long range correlation and long range*

291   *cross-correlation*

292
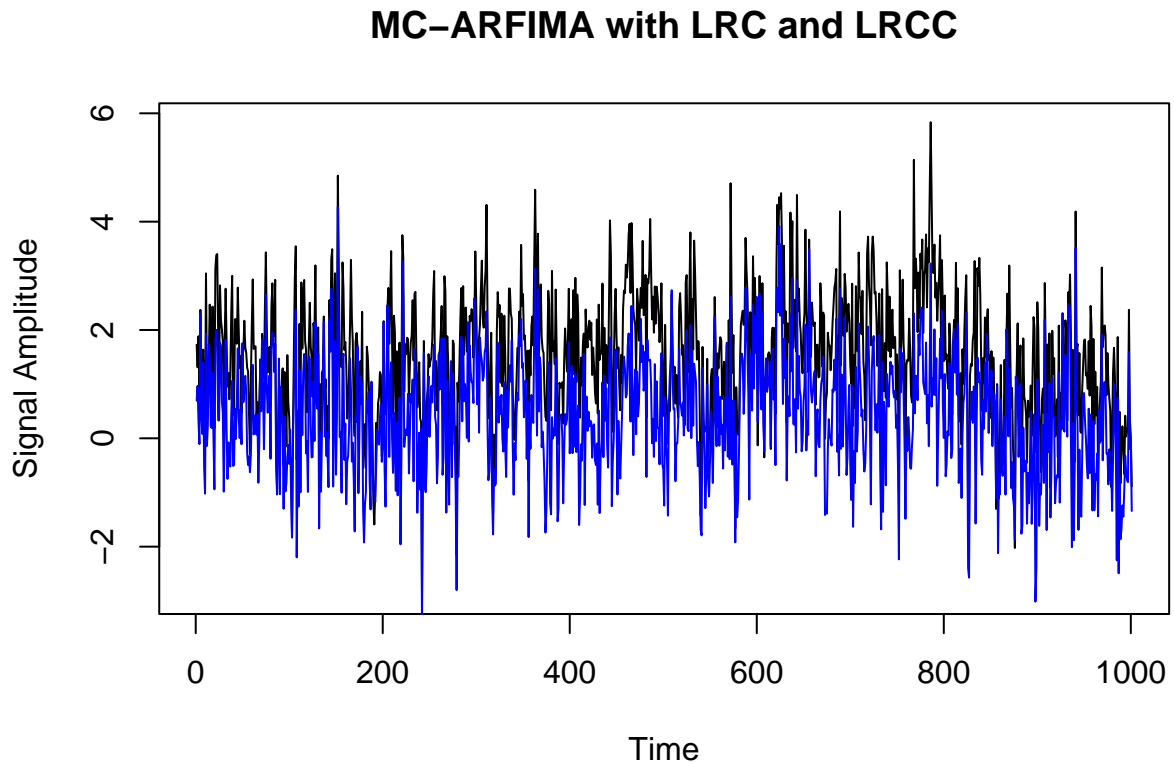
293   As can be seen in Figure 7, the simulated time series, although quite noisy, appear to

294   covary over time with similar trends. To perform the `dcca()` on these time series, we use

295   the code below, where we first define the `scales` using the `logscale()` function described

296   earlier along with the `dcca()` function itself.

```
scales <- logscale(scale_min = 10, scale_max = 1000, scale_ratio = 1.1)


dcca.out.arfima <- dcca(sim1[,1], sim1[,2], order = 1, scales = scales)
```

297   Next, we visualize the output of DCCA in Figure 8. We observe that, as expected,

298   the correlation between the MC-ARFIMA processes are consistently high (all ρ's > .8) and

299   continue to be high at increasing time scales.
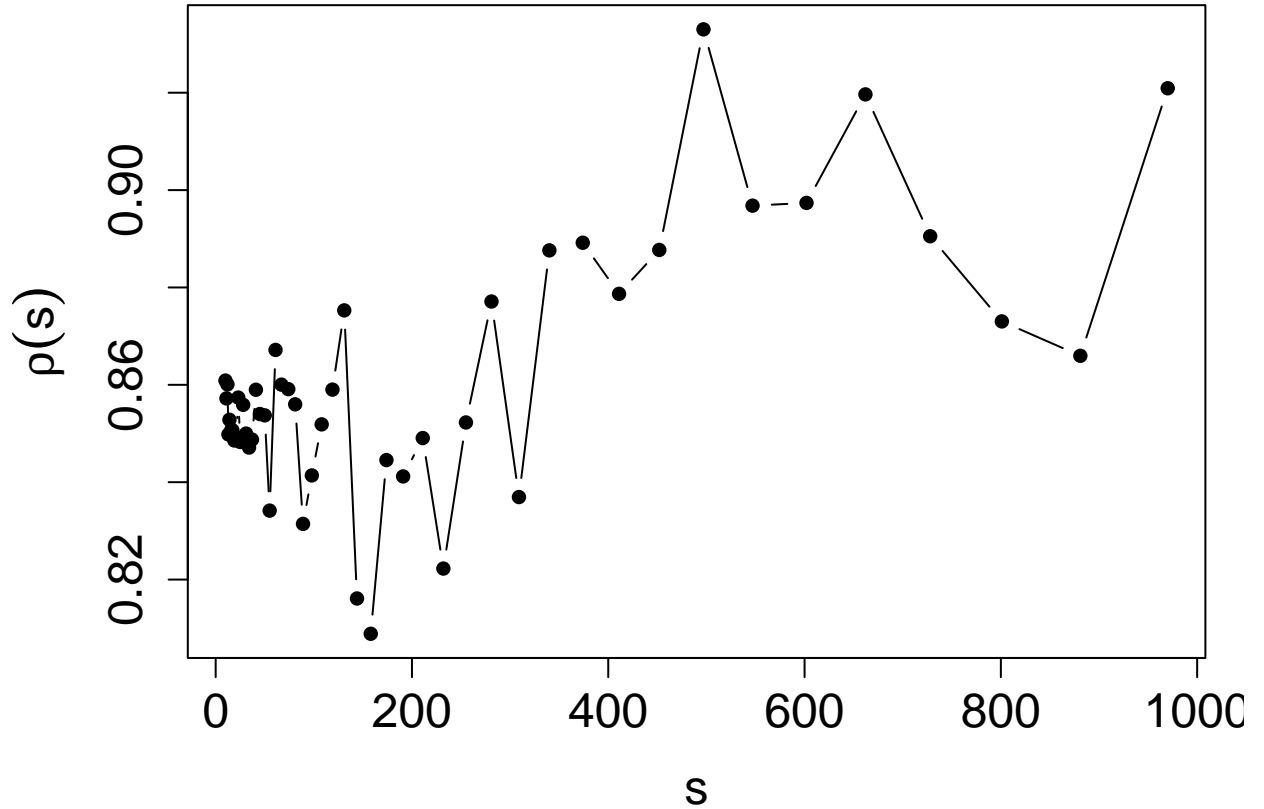
300   **Figure 8**

301   *DCCA output for long range correlation and long range cross-correlation*

302

303   Figure 8 is difficult to interpret on its own. To address this, we demonstrate an

304   additional plot and analysis feature of `dcca()` by modifying the above code as shown

305   below `ci = TRUE`. Loess smoothing can also be applied to both $\rho(s)$ and its confidence

306   intervals using `loess.rho = TRUE` and `loess.ci = TRUE`. Those latter options are useful

307   for reducing the impact of increasing variance on estimates of $\rho(s)$ at large scales (Likens et

308   al., 2019b). Note though that a much larger set of calculations takes place and may take

309   several seconds up to several minutes (for long time series) to complete. This method is

310   shown in Figure 9. Importantly, it shows us that there is evidence of long range

311   cross-correlations as there $\rho(s)$ for all scales are outside of the surrogate confidence interval.

312   **Figure 9**

313   *DCCA output for long range correlation and long range cross-correlation with Loess*

314   *smoothing on estimates and a surrogate confidence interval*

315
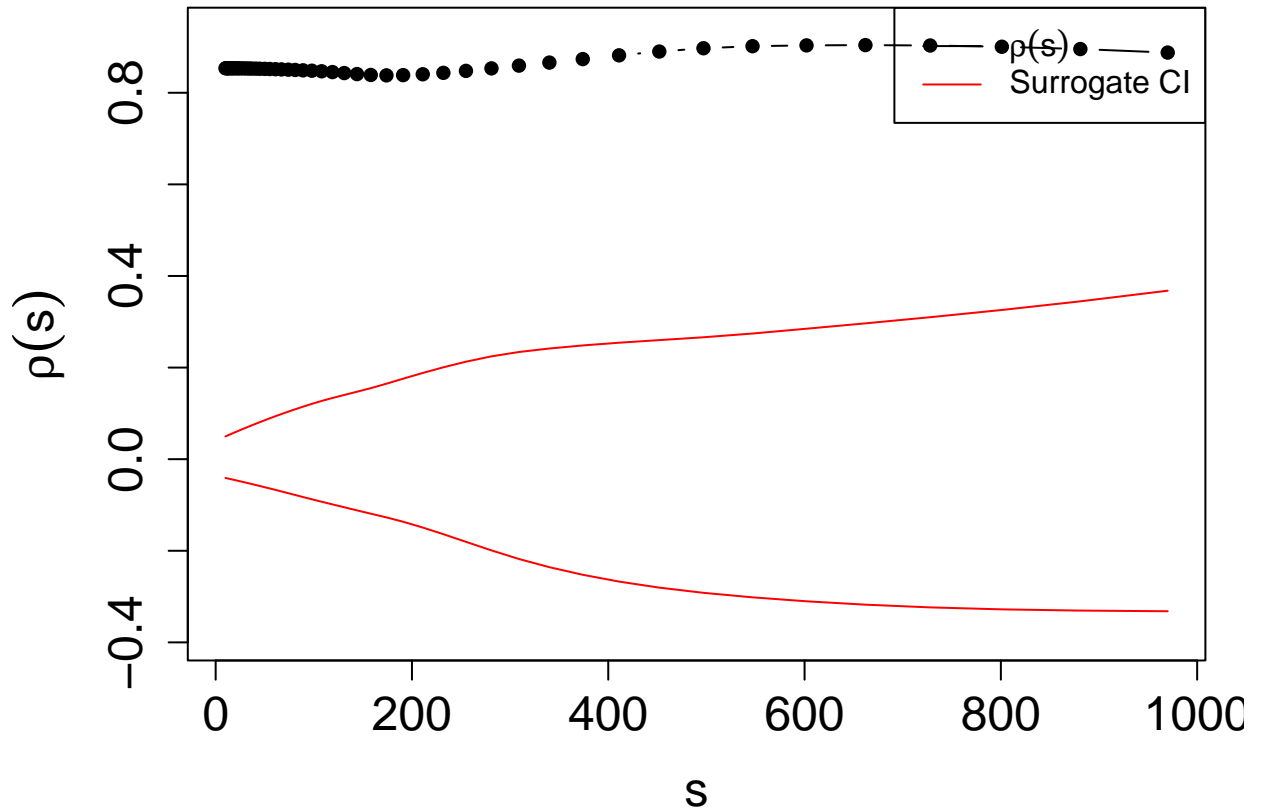
316   As a point of comparison, we can generate a time series in contrast with this that

317   exhibits processes with LRC and short-range cross-correlation (SRCC) using the code

318   below. In contrast to the previous DCCA analysis, Figure 10 shows a signal that begins

319   with a high cross-correlation (ρ's $\approx$ .6), but that begins to deviate and trend substantially

320   lower at increasing scale sizes with ρ entering the confidence interval containing 0. In fact,

321   based on the plotted confidence intervals, the correlation between the two series becomes

322   non-significant from a conventional standpoint.

323   **Figure 10**

324   *DCCA output for long range correlation and short range cross-correlation including*

325   *smoothing and a surrogate confidence interval*

326
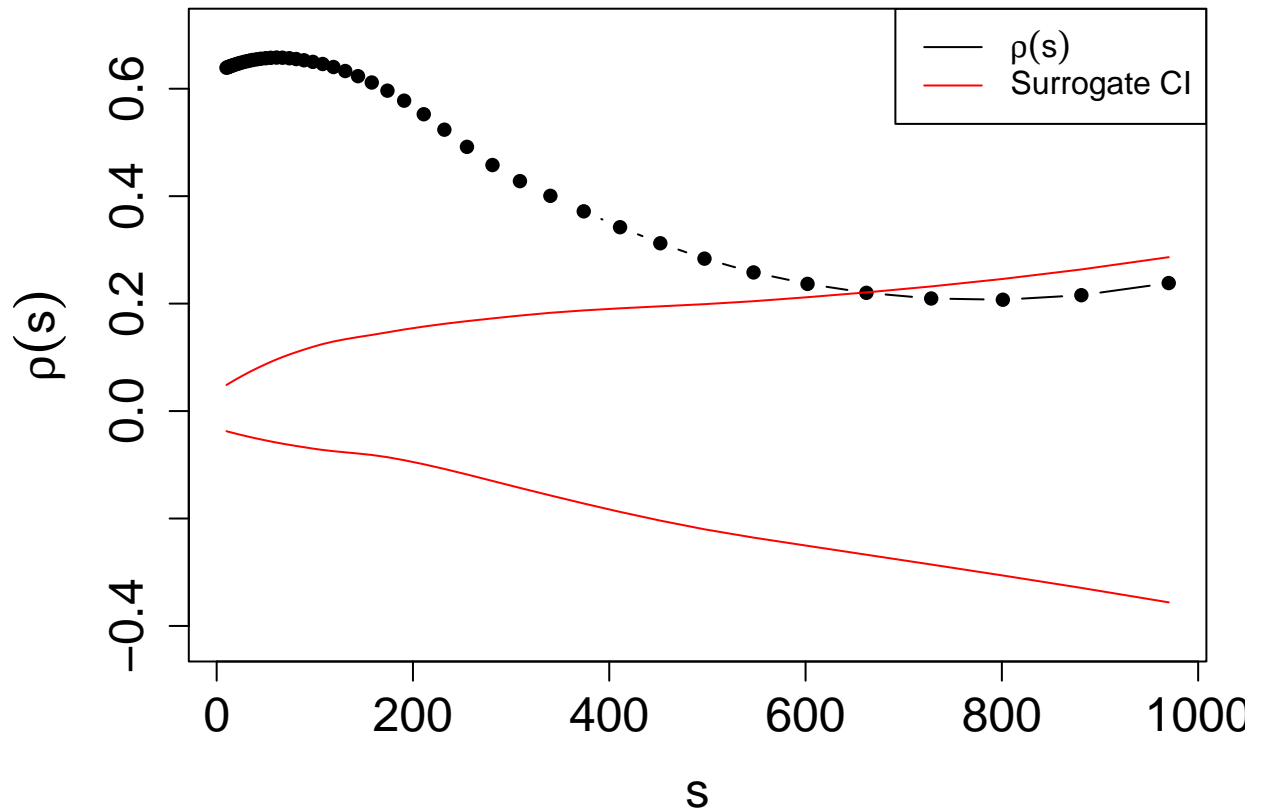
Turning next to the empirical balance data, we apply DCCA to the differenced COPx

and COPy data for the firm and foam platforms. We again set appropriate values for

`scales` and apply the `dcca()` function to the pair of time series.

Figure 11

DCCA output for empirical COPx and COPy balance data for the eyes open while

standing on the firm surface (top) and foam surface (bottom)
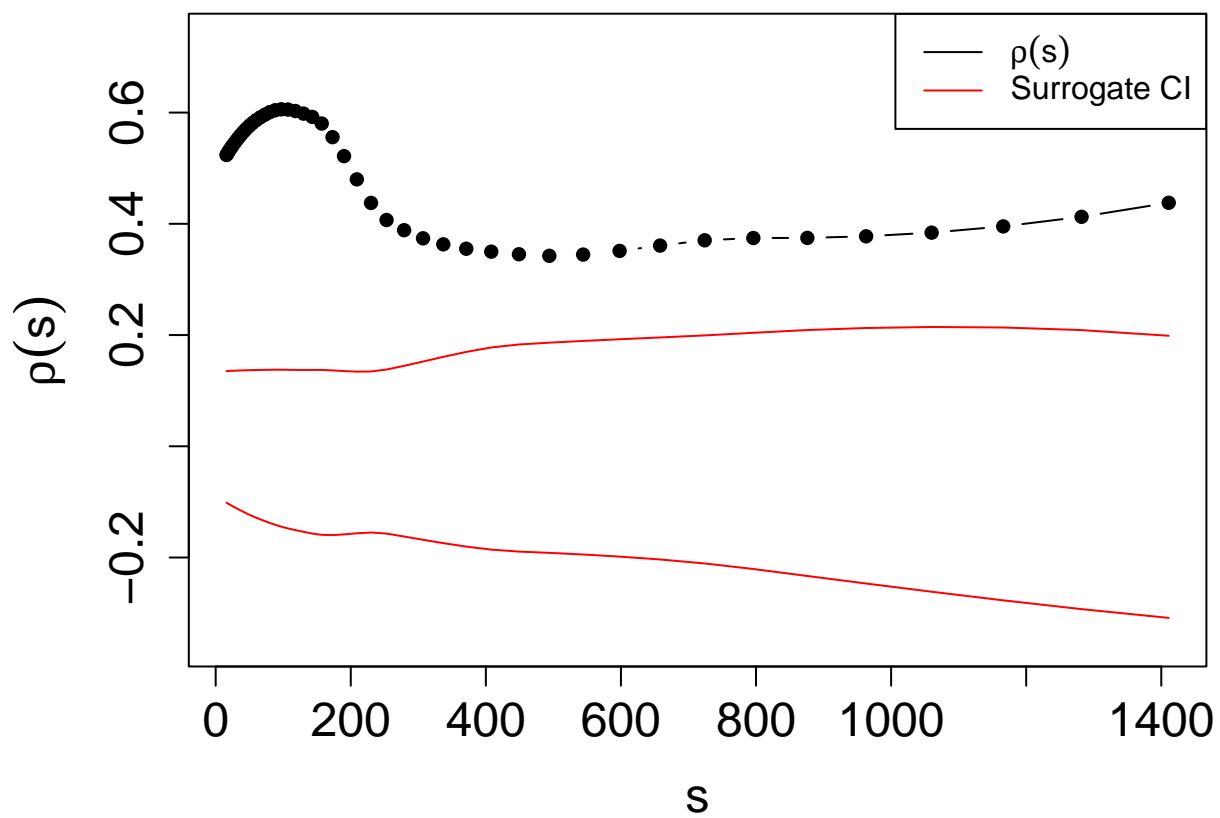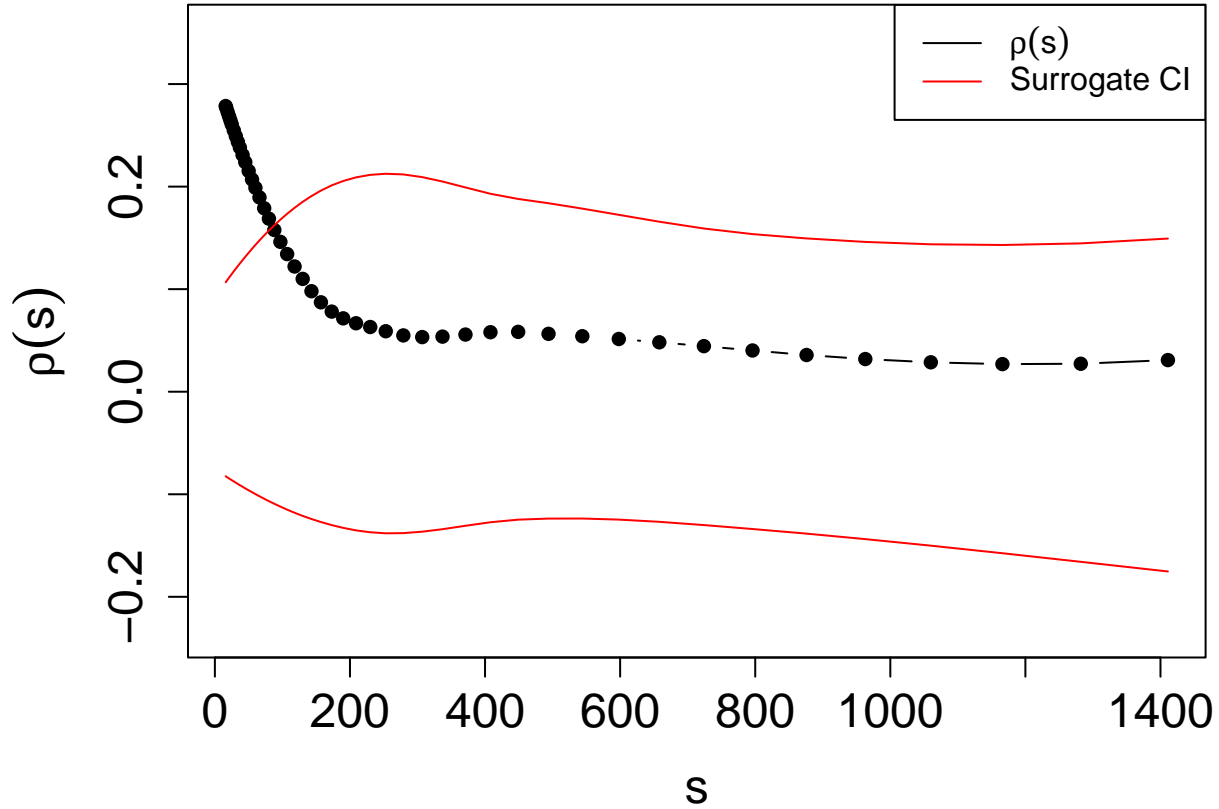
In examining the output from these analyses, Figure 11 shows a clear difference between the two conditions. First, in the firm platform example, the $\rho(s)$ values reach an order of magnitude greater than in the foam condition with the max $\rho(s) = 0.73$ compared to 0.35 for the foam condition. Second, we observe for the foam example, that the time scale of maximum correlation is 73, which is a larger time scale when compared to the foam example, which had a maximum correlation at scale 16. Third, the pattern of change in correlation across scales is slightly different. The firm example is higher overall; it starts relatively low at very small time scales before a rapid increase and then steady decrease before stabilizing at increasingly larger scales. By contrast, the foam example has relatively lower overall correlation values, the smallest scale is the highest followed by a steady decrease and then also stabilizing at larger scales. Lastly, we can also derive statistical conclusions because, in the firm condition, the two series are correlated at all scales, whereas the series are only correlated beyond chance at the smaller scales in the foam

348 condition.

349 **Multiscale Regression Analysis.**   Multiscale regression analysis (MRA) is a

350 further generalization of DCCA that brings the analyses into a predictive, regression

351 framework (Kristoufek, 2015b). The key questions that can be answered by it are: a) *How*

352 *does the influence of one time series on another time series change as a function of scale?*

353 and b) *What is/are the dominant (time) scale(s) of influence of one time series on another*

354 *time series?* The algorithm is largely the same as DCCA, with a key difference being that

355 instead of estimating scale-wise symmetric correlation coefficients, leveraging methods of

356 Ordinary Least Squares (OLS) regression, asymmetric β coefficients are estimated

357 (Kristoufek, 2015b; Likens et al., 2019b) according to the following equation:

$$\beta(s) = \frac{F_{xy}(s)}{F_x^2(s)}$$

358 The $\beta(s)$ equation differs from the $\rho(s)$ equation only in the denominator where $F_x^2(s)$

359 is the average squared residual at each scale and $F_x y(s)$ is still the scale-wise covariance.

360 ***MRA Examples.***   Considering the LRC and LRCC simulations used for DCCA,

361 we can examine whether the scale-wise fluctuations of one variable can predict the

362 scale-wise fluctuations of the other using `mra()`. As with a traditional regression approach,

363 we will use one of our variables as our predictor (x_t) and the other as our outcome (y_t). In

364 the example below, we again first define our logarithmically spaced scales. We then apply

365 the `mra()` function to the two simulated time series. In this case, it's important to specify

366 which is variable is `x` (the predictor) and which is `y` (the outcome).

```
scales <- logscale(scale_min = 10, scale_max = 1000, scale_ratio = 1.1)


mra.out <- mra(x = sim1[,1], y = sim1[,2], order = 1, scales = scales)
```

367 We can then visualize these results as shown below in Figure 12. Generally, we

observe that the β coefficients are relatively stable at increasing time scales with a general,

perhaps quadratically increasing trend. Here it is also important to investigate the change

in R^2 as well as the t-values. Below we see that the R^2 is quite high at most of the time

scales with $R^2_{min} = 0.67$ and $R^2_{max} = 1.85$ and all $\beta(s)$ exceed the confidence intervals,

implying conventional statistical significance. So between these two component ARFIMA

processes, the output of MRA shows that much of the scale specific variance in y_t is

explained and predicted by x_t.

Figure 12

MRA output for long range correlation and long range cross-correlation
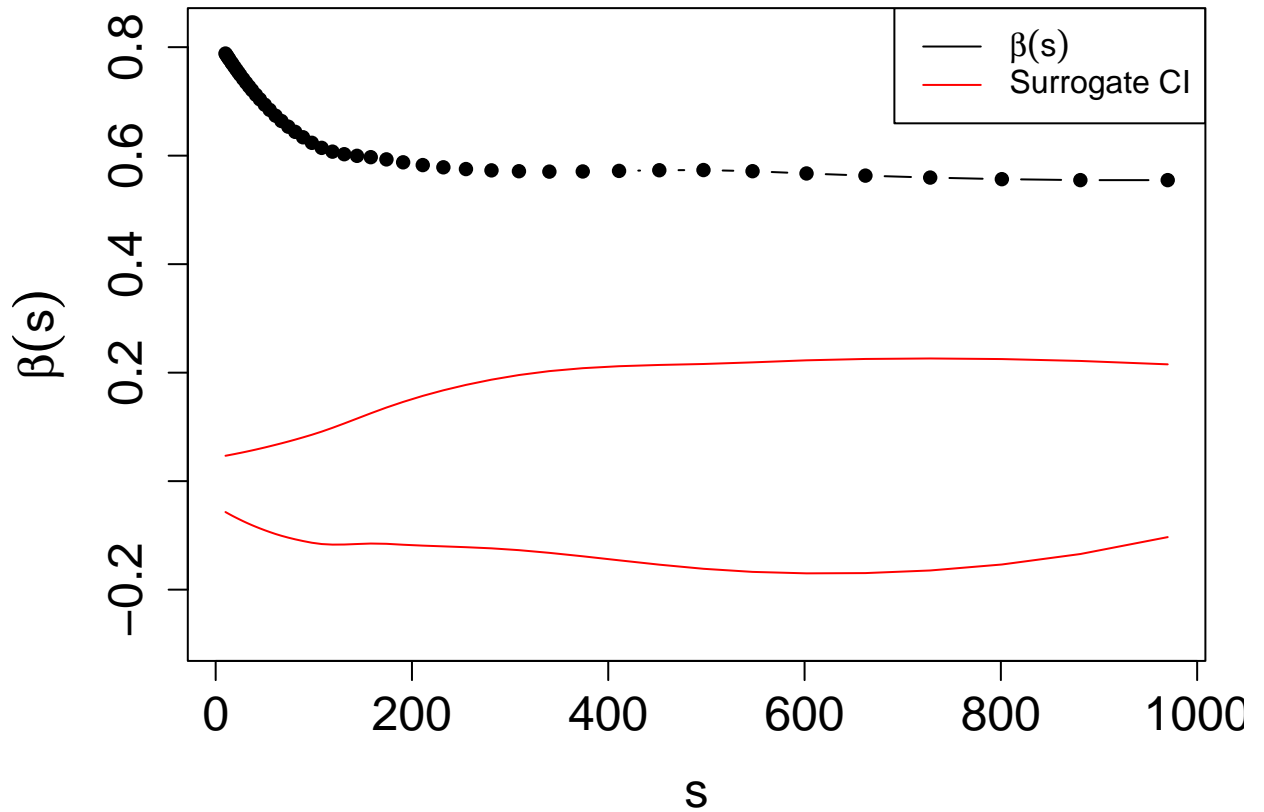
Turning next to the empirical balance data, we can determine whether postural

adjustments in the COPx are predictive of adjustments in COPy, and vice versa. This

means that we use the `mra()` function two times and reverse the order of entry for the x

and y arguments to allow for determining the degree to which each signal can predict the

382   other across scales. In Figure 13 below, we see the resulting β's we observed for the the

383   balance data on the firm surface. Notably, the COPx predicting COPy (max $\beta = 0.19$) has

384   noticeably smaller β values compared to COPy predicting COPx (max $\beta = 3.25$). Notice

385   as well how Figure 13 (bottom), where adjustments in the y dimension are predicting

386   adjustments in the x dimension, resembles the DCCA plot for this analysis (see Figure 11).

387   Given the asymmetry in the magnitude of the βs, this example suggests that postural

388   adjustments in the y dimension appear to be driving changes in the x dimension. And,

389   there is a clear time scale where this relationship is strongest at scales = 55, implying a

390   dominant mode of coordination between mediolateral and anterioposterior control

391   processes.

392   **Figure 13**

393   *MRA output for balance data on foam surface with COPx predicting COPy (top) and*

394   *COPy predicting COPx (bottom).*

395
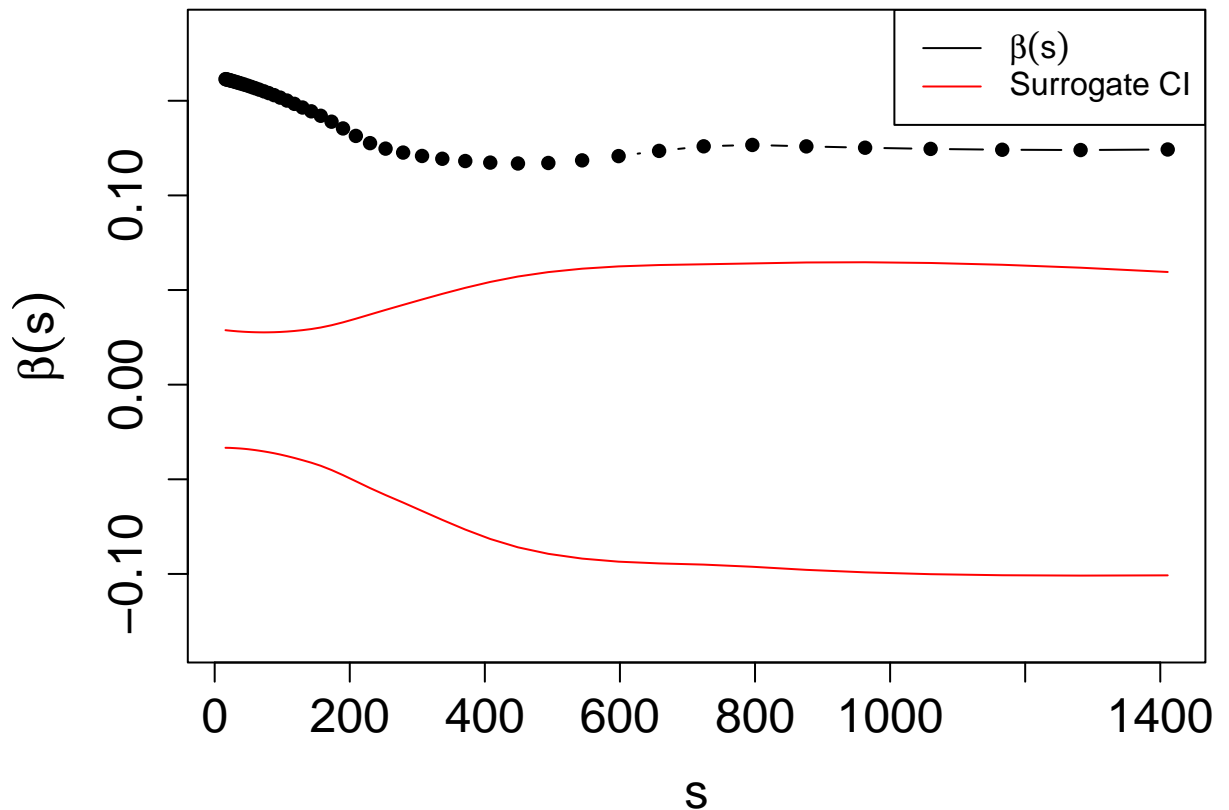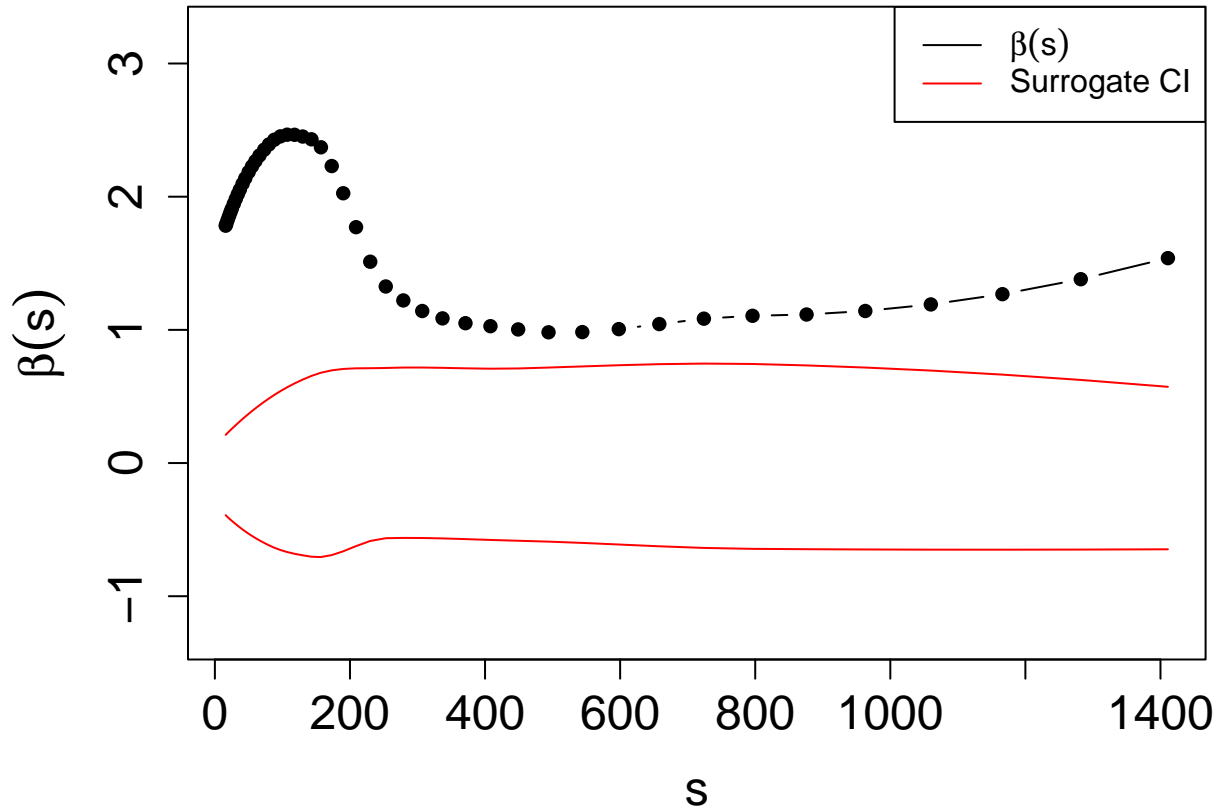
Surrogate Methods

In all of the above methods, one gets either a single estimate of a parameter (e.g., α) or a range of estimates (e.g., $\rho(s)$, $\beta(s)$). While those estimates are meaningful in and of themselves, it is common practice to perform some form of null hypothesis test regarding the estimate(s). These are generally referred to as surrogate methods (Kantz & Schreiber, 2003). We present several options here that could be ranked in terms of increasing levels of rigor: randomized surrogates, iterative amplitude adjusted Fourier transformed (IAAFT) surrogates, and model-based surrogates.

Randomized Surrogates.   Randomized surrogates generally involve randomly shuffling the order of values of a time series. The idea is generally that the temporal structure is destroyed, yet the other features of the time series still exist (Kantelhardt et al., 2002). The confidence intervals for all of our plotting methods use this technique. Note

409 that additional options exist along these lines (see for example (Dumas, Nadel, Soussignan,

410 Martinerie, & Garnero, 2010)). The key comparison here would be to compare the

411 estimates extracted from a given analysis (e.g., DFA) on the observed sample of data with

412 the estimates derived from an equally sized sample of the surrogate series (Kantz &

413 Schreiber, 2003; Moulder, Boker, Ramseyer, & Tschacher, 2018; Wiltshire, Steffensen, &

414 Fiore, 2019).

```
rand.surr <- permute::shuffle(pink.noise)


dfa.rand.surr <- dfa(x = rand.surr, order = 1, verbose = 1,
scales = scales, scale_ratio = 1.1)
```

415   Randomizing the pink noise time series, which originally exhibited long range

416 correlation ($\alpha = 0.82$), and performing DFA on it, now provides an estimate of $\alpha = 0.55$,

417 which is consistent with a random or white noise process. These values are clearly

418 different, however, performing inferential statistics on a sample of observed estimates

419 compared to surrogate estimates would provide compelling evidence that the temporal

420 dynamics suggested by the observed estimates are different than those derived from a

421 random process.

422 **Iterative Amplitude-Adjusted Fourier Transform Surrogates (IAAFT).**

423 The IAAFT algorithm was originally developed as a way to discern whether nonlinearity is

424 a feasible explanation for time series patterns (Schreiber & Schmitz, 1996). More recently,

425 it was proposed as a technique to determine if multifractal indices suggest interaction

426 across scales (Ihlen & Vereijken, 2010). Like with randomized shuffling, estimates derived

427 from IAAFT surrogates should be also be different from the estimates derived from the

428 empirical time series. Although in this case, the comparison is typically made between the

429 multifractal spectra of the observed time series, and the typical spectrum derived

430 empirically from a set of IAAFT surrogate series.

431 In the code below, we provide an example for generating IAAFT surrogates using the

432 `iaafft()` function in the package. One enters the `signal`, which is the observed time

433 series, and `N`, the number of surrogates to generate. There are a number of options here,

434 but a common number of surrogates is 19 (Kantz & Schreiber, 2003), which allows one to

435 establish a 95% confidence interval. In practice, surrogates are generated from each

436 observed time series. Here we illustrate the process using only a single time series: the

437 multifractal signal used previously in the MFDFA example. Then we use the same

438 parameters for the `mfdfa()` function, but apply it to all of the IAAFFT surrogates. Note

439 also that surrogate analysis is 'built-in' to our plot functions within the package as well

440 with options to return the relevant empirically derived confidence intervals.

```
iaafft.surr <- iaafft(fractaldata$multifractal, N = 19)


iaafft.surr.out <- apply(iaafft.surr, MARGIN = 2, FUN = mfdfa,
q = c(-5:5), order = 1, scales=scales, scale_ratio = 2)
```

441 Assuming we were using IAAFFT to compare the multifractal width (W) between

442 the observed signal and the surrogate signals, recall that the observed width was $W_{multi} =$

443 1.36. Now, we can calculate the average multifractal width across all of the generated

444 surrogates and we observe that $W_{surr} = 0.61$, which is narrower than the spectrum from

445 the multifractal signal. In practice, there are many surrogate options (Moulder et al.,

446 2018), but, again, inferential statistics are commonly performed to compare observed

447 estimates to the surrogate estimates to bolster evidence of the inferred dynamics.

448 **Model-based Surrogates.** Surrogates can also be generated when a theoretical

449 model exists that explains the data generating process for the observed time series.

450 Well-defined mathematical models of this nature are rare in behavioral sciences, but useful

451 because they allow for more targeted and (potentially) realistic hypothesis testing of the

452 underlying dynamics and how they might change due to experimental constraints. We do

⁴⁵³ not provide a worked out example of such processes, but readers can consult cited papers

⁴⁵⁴ for examples of this kind (Delignières et al., 2011a; Likens et al., 2019b; Roume et al.,

⁴⁵⁵ 2018).

General Discussion

⁴⁵⁷   In this manuscript, we provided details about the first version of a new R package

⁴⁵⁸ aimed at bringing together a number of fractal methods that we and other researchers have

⁴⁵⁹ found useful in analyzing a range of behavioral and physiological data. Indeed, these

⁴⁶⁰ collective methods have found utility in virtually every area of science. Despite that reach,

⁴⁶¹ many researchers are still not aware of these methods or lack software for their

⁴⁶² implementation. This `fractalRegression` package is our effort to bridge those gaps by

⁴⁶³ demonstrating each of several methods first with simulated data, followed by equivalent

⁴⁶⁴ demonstrations with human movement data (only one of many possible use cases). This

⁴⁶⁵ allows the reader to see both the 'best case' scenario as well as the idiosyncrasies that rear

⁴⁶⁶ their heads when we transition from the pristine world of simulation to the noisiness

⁴⁶⁷ inherent in empirical human behavioral data.

⁴⁶⁸   Taken together, these methods allow researchers to examine, in univariate time series,

⁴⁶⁹ the magnitude and direction of long range correlation and/or how that magnitude and

⁴⁷⁰ direction might change over time. In bivariate cases, these methods allow for determining:

⁴⁷¹ (1) how the correlation between time series changes as a function of scale and (2) what the

⁴⁷² dominant (time) scale(s) of coordination are. Or, relatedly, one can investigate how the

⁴⁷³ influence of one time series on another changes as a function of the scale of observation

⁴⁷⁴ while potentially identifying the dominant (time) scale(s) of influence. Thus, these methods

⁴⁷⁵ provide general value and can answer several types of questions on many types of data. To

⁴⁷⁶ do so effectively requires careful and appropriate application, though. We next discuss some

⁴⁷⁷ of these considerations while also referring the reader to other helpful tutorial material.

478   ***Practical considerations for univariate methods (DFA, MFDFA).*** We

479   recommend a few points of consideration in conducting DFA and MFDFA. One is to be

480   sure to evaluate whether there are cross-over points in the log scale-log fluctuation plots

481   (Kantelhardt et al., 2001; Likens et al., 2015; Likens & Stergiou, 2020; Peng et al., 1994;

482   Perakakis, Taylor, Martinez-Nieto, Revithi, & Vila, 2009). Cross-over points (or a visible

483   change in the slope as a function of scale) indicate that a simple mono-fractal

484   characterization does not sufficiently characterize the data. If cross-over points are evident,

485   we recommend proceeding to estimate the two scaling regions with a piece-wise regression

486   (as we showed for the empirical DFA example). Note, however, that for the empirical

487   MFDFA example above, we did not parse the signal for piece-wise MFDFA although some

488   efforts have been conducted for decomposing crossovers in multifractal signals (Nagy,

489   Mukli, Herman, & Eke, 2017). Other suggestions are to only analyze a single linear region

490   (Ihlen, 2012). Regardless, more research is needed to understand the implications of

491   crossover phenomena with respect to the more complicated fluctuation functions of

492   MFDFA.

493   While it is common to use only linear detrending with DFA, this is not necessarily

494   the best practice. Instead, a more rigorous approach requires inspection of trends in the

495   data to determine if a higher order polynomial would be more appropriate for detrending.

496   There are certainly instances in the literature where DFA fluctuation plots show signs of

497   curvilinearity (Delignières et al., 2011b). Such curvilinearity could be interpreted as

498   representing an inflection point. In such cases, one can compare the DFA output for

499   different polynomial orders (Kantelhardt et al., 2001) to determine if a genuine inflection

500   point is present or if nonlinearity in DFA and MFDFA emerges due to unadressed

501   nonlinear trends in the original series (Likens et al., 2019b). Indeed, one is not simply

502   limited to OLS detrending with polynomials. Many other propositions have been

503   introduced to generalize the idea of detrending function to other models such as moving

504   averages (Xu et al., 2005) and even non-parametric techniques like emprical mode

505 decomposition (Qian, Gu, & Zhou, 2011). Those and other more 'exotic' detrending

506 techniques will be featured in future releases of this package (see Development Plan below).

507   Another important matter concerns the length of the time series being analyzed.

508 Unfortunately, all of the methods presented in this manuscript are relatively data hungry.

509 The general trend is that estimation error of various quantities detailed above grows

510 dramatically as time series length decreases (Delignieres et al., 2006). That work and other

511 simulation studies have revealed that reliable estimates of fractal quantities requires a

512 minimum length of the time series of ~512 observations although larger is better

513 (Delignieres et al., 2006; Likens et al., 2019b). That recommendation holds true for both

514 univariate and bivariate cases, alike. If multiple time series are to be compared, then it's

515 also important that they have matching lengths. Relatedly, general recommendations for

516 choosing the min and max scale are a minimum scale of 10 and a maximum scale of N/4,

517 where N is the total number of observations in the signal. See Eke, Herman, Kocsis, and

518 Kozak (2002) and Gulich and Zunino (2014) for additional considerations but also keep in

519 mind specific research areas may also have other criteria (Damouras, Chang, Sejdić, &

520 Chau, 2010; Marmelat & Meidinger, 2019).

521   ***Practical considerations for bivariate methods (DCCA, MRA).***   As

522 suggested above, all of the above considerations also apply in the bivariate case such as

523 recommendations for length, scales sizes, and detrending. This is not surprising given that

524 those methods share a common mathematical girding. However, given that the estimands

525 in DCCA and MRA are qualitatively different that those in DFA and/or MFDA, there are

526 likewise some unique issues as well. Regarding time series length, previous research has

527 shown that $\widehat{\beta}(s)$ is unbiased regardless of series length and underlying distribution;

528 however, it's variance increases dramatically with decreasing time series length, especially

529 for large time scales (Likens et al., 2019b). This has important consequences for evaluation

530 of statistical significance of $\widehat{\beta}(s)$ for large s. Namely, ever larger $\widehat{\beta}(s)$ may be needed to

531 exceed conventional levels of significance (e.g., $p < .05$). While $\widehat{\beta}(s)$ is unbiased, even for

532 non-Gaussian, time series, that property does not hold in the presence of trends (e.g.,

533 linear, quadratic) or nonstationarity. In both those instances, $\widehat{\beta}(s)$ becomes positively

534 biased, which could imply spurious positive relationships between series if not addressed.

535 In both those instances, one promising remedy seems to be higher order detrending

536 polynomials (e.g., quadratic, cubic). This remedy also seems to apply, even when the

537 underlying increments of nonstationary processes have non-Gaussian distributions.

538 Therefore, it is of utmost importance to inspect time series for strong time trends (e.g., via

539 OLS regression with various powers of time as a predictors) and nonstationarity (e.g.,

540 Dickey-Fuller tests) so that a sufficient order detrending function can be selected for use in

541 the analysis.

542 ***Development Plan.*** The current release version of the `fractalRegression`

543 package features all of the functions presented in Table 1. Other functions are also

544 currently available for research and development but should be considered "works in

545 progress" as they require additional testing but will be elevated in future releases of the

546 package. For example, lagged versions of DCCA and MRA, known as Detrended Lagged

547 Cross Correlation Analysis (DLCCA) or Multiscale Lagged Regression Analysis (MLRA)

548 respectively, are forthcoming. Those methods pose some new challenges for scientists. For

549 example, choosing an optimal time lag requires careful consideration in this multiscale

550 context. Time lag selection can, in part, be based on theoretically motivated temporal

551 distance in which the two processes are expected to be related. However, new research

552 questions may not carry that level of specificity. In this case, it can also be a process of

553 trial and error to determine the maximum lag to include in the analysis using visual

554 inspection. More rigorously, there are other methods for determining a maximum time lag

555 using a critical value that is dependent on time scales (Shen, 2015); we expect those

556 techniques might be generalized for MLRA as well. Table 3 below shows our initial plan for

557 functions to include in future iterations of the package. Of course, as the package becomes

558 more utilized, new ideas and resources may be come available to build on the current

functionality. To that end, we welcome feature requests and collaborations to grow the package to meet the diverse needs of the scientific community.

Table 3

Overview of development plan for `fractalRegression` *package*

Conclusion

In this paper, we advance the `fractalRegression` R package as a new tool for behavioral, cognitive, and social scientists from varied backgrounds and provide examples of its use on simulated and empirical data. We hope that in collating these methods, and making them efficient, that they will be more accessible and systematically utilized across disciplines. There are many unanswered questions about these methods and the complex dynamics they characterize Our hope is that this work inspires future efforts that not only apply these methods, but that also expand on them to further our understanding of the complexities of multiscale interactions in dynamic systems.

Appendix 1: Fundamental Equations

In this appendix, we provide the corresponding equations given for computation of the methods presented in this manuscript and implemented in our package. There is a natural progression from DFA to DCCA and MRA (Kristoufek, 2015b; Likens et al., 2019b). That progression is given below, starting with:

DFA

$$F_X = \sqrt{\frac{\sum_{j-1}^{T-s+1} f_X^2(s,j)}{T-s}}$$

where

$$f_X^2(s,j) = \frac{\sum_{k=j}^{j+s-1}(X_k - \widehat{X}_{k,j})}{s-1}$$

DCCA

582 $$F_Y = \sqrt{\frac{\sum_{j-1}^{T-s+1} f_Y^2(s,j)}{T-s}}$$

583 where

584 $$f_Y^2(s,j) = \frac{\sum_{k=j}^{j+s-1}(Y_k - \widehat{Y}_{k,j})}{s-1}$$

585 and the scale-wise covariance is estimated as:

586 $$f_{XY}^2(s,j) = \frac{\sum_{k=j}^{j+s-1}(X_k - \widehat{X}_{k,j})(Y_k - \widehat{Y}_{k,j})}{s-1}$$

587 which forms the basis for the scale-wise correlation coefficient estimated as:

588 $$\rho(s) = \frac{F_{XY}^2(s)}{F_X(s)F_Y(s)}$$

589 and for the multi-scale regression coefficients, we replace the denominator in the $\rho(s)$

590 equation with scale-wise variance of the predictor to estimate the scale-wise regression

591 coefficient from regression Y_t on X_t as:

592 $$\widehat{\beta}(s) = \frac{F_{XY}^2(s)}{F_X^2(s)}$$

593 and where the variance of $\widehat{\beta}(s)$ is:

594 $$\sigma_{\widehat{\beta}(s)}^2 = \frac{1}{T-2} \times \frac{F_u^2(s)}{F_Y^2(s)}$$

595 and the scale-wise residual variance, $\widehat{F}_u^2(s)$ is estimated by applying the DFA

596 algorithm to all scale-wise residuals, $\widehat{u}_t(s)$ as:

597 $$\widehat{u}_t(s) = y_t - x_t\widehat{\beta}(s) - \overline{y_t - x_t\widehat{\beta}(s)}.$$

598 MFDFA

599 The foundational equation for MFDFA is similar to that of DFA, following notation

600 from (Kantelhardt et al., 2002), we have

601 first a profile function for a given time series, $y(t)$

602 $$Y(i) = \sum_{k=1}^{i}[x(k) - \bar{x}] \quad \text{for} \quad i = 1, 2, ..., N,$$

603 where $x(i)$ is the original time series, $\bar{x}$ is its mean, and N is the length of the time

604 series.

As in DFA we divide the profile function into N_s non-overlapping windows of length
s, and within each window, we fit a polynomial function of order m to remove trends and
compute the variance

$F^2(v, s) = \frac{1}{s} \sum_{i=1}^{s} Y[(v-1)s + i]^2$

for each segment, $v, v = 1, 2, ...N_s$ and

$F^2(v, s) = \frac{1}{s} \sum_{i=1}^{s} \{Y[N - (v - N_s)s + i] - y_v(i)\}^2$

where $y_v(i)$ is fitting polynomial of order m. Next, we average over all segments to
obtain the qth order fluctuation function

$F_q(s) = \{\frac{1}{2N_s} \sum_{v=1} 2N_s[F^2(v, s)]^{q/2}\}^{1/q}$

where q can take any real value. Given that $F_q(s)$ generalizes the DFA fluctuation
function, F_X, given above, we are interested in understanding how $F_q(s)$ changes with
s which we investigate with log-log regressions of those quantities where we expect

$F_q(s) \sim s^{h(q)}$

where h(q) is the generalized Hurst exponent. Other fractal quantities can be
computed by transformations of $h(q)$. See (Kantelhardt et al., 2002) for details.

Acknowledgments

624   **References**

625   Bak, P., Tang, C., & Wiesenfeld, K. (1987). Self-organized criticality: An

626   explanation of the 1/f noise. *Physical Review Letters*, *59*(4), 381–384.

627   https://doi.org/10.1103/PhysRevLett.59.381

628   Bianchi, S. (2020). Fathon: A python package for a fast computation of detrendend

629   fluctuation analysis and related algorithms. *Journal of Open Source Software*,

630   *5*(45), 1828.

631   Cavanaugh, J. T., Kelty-Stephen, D. G., & Stergiou, N. (2017). *Multifractality,*

632   *Interactivity, and the Adaptive Capacity of the Human Movement System: A*

633   *Perspective for Advancing the Conceptual Basis of Neurologic Physical Therapy.*

634   Retrieved from https:

635   //www.ingentaconnect.com/content/wk/npt/2017/00000041/00000004/art00007

636   Collins, J. J., & De Luca, C. J. (1993). Open-loop and closed-loop control of

637   posture: A random-walk analysis of center-of-pressure trajectories. *Experimental*

638   *Brain Research*, *95*(2), 308–318. https://doi.org/10.1007/BF00229788

639   Damouras, S., Chang, M. D., Sejdić, E., & Chau, T. (2010). An empirical

640   examination of detrended fluctuation analysis for gait data. *Gait & Posture*,

641   *31*(3), 336–340. https://doi.org/10.1016/j.gaitpost.2009.12.002

642   Davis, T. J., Brooks, T. R., & Dixon, J. A. (2016). Multi-scale interactions in

643   interpersonal coordination. *Journal of Sport and Health Science*, *5*(1), 25–34.

644   https://doi.org/10.1016/j.jshs.2016.01.015

645   Delignieres, D., Ramdani, S., Lemoine, L., Torre, K., Fortes, M., & Ninot, G.

646   (2006). Fractal analyses for 'short' time series: A re-assessment of classical

647   methods. *Journal of Mathematical Psychology*, *50*(6), 525–544.

648   https://doi.org/10.1016/j.jmp.2006.07.004

649   Delignières, D., Almurad, Z. M. H., Roume, C., & Marmelat, V. (2016).

650   Multifractal signatures of complexity matching. *Experimental Brain Research*,

651 *234*(10), 2773–2785. https://doi.org/10.1007/s00221-016-4679-4

652 Delignières, D., & Torre, K. (2009). Fractal dynamics of human gait: A

653   reassessment of the 1996 data of Hausdorff et al. *Journal of Applied Physiology*,

654   *106*(4), 1272–1279. https://doi.org/10.1152/japplphysiol.90757.2008

655 Delignières, D., Torre, K., & Bernard, P. L. (2011a). Interest of velocity variability

656   and maximal velocity for characterizing center-of-pressure fluctuations. *Science*

657   *& Motricité*, (74), 31–37. https://doi.org/10.1051/sm/2011107

658 Delignières, D., Torre, K., & Bernard, P.-L. (2011b). Transition from Persistent to

659   Anti-Persistent Correlations in Postural Sway Indicates Velocity-Based Control.

660   *PLOS Computational Biology*, *7*(2), e1001089.

661   https://doi.org/10.1371/journal.pcbi.1001089

662 Delignières, D., Torre, K., & Lemoine, L. (2008). Fractal models for event-based

663   and dynamical timers. *Acta Psychologica*, *127*(2), 382–397.

664   https://doi.org/10.1016/j.actpsy.2007.07.007

665 Dumas, G., Nadel, J., Soussignan, R., Martinerie, J., & Garnero, L. (2010).

666   Inter-Brain Synchronization during Social Interaction. *PLOS ONE*, *5*(8),

667   e12166. https://doi.org/10.1371/journal.pone.0012166

668 Eddelbuettel, D., & Francois, R. (2011). Rcpp: Seamless R and C++ Integration.

669   *Journal of Statistical Software*, *40*(1), 1–18.

670   https://doi.org/10.18637/jss.v040.i08

671 Eddelbuettel, D., & Sanderson, C. (2014). RcppArmadillo: Accelerating R with

672   high-performance C++ linear algebra. *Computational Statistics & Data*

673   *Analysis*, *71*, 1054–1063. https://doi.org/10.1016/j.csda.2013.02.005

674 Eke, A., Herman, P., Kocsis, L., & Kozak, L. R. (2002). Fractal characterization of

675   complexity in temporal physiological signals. *Physiological Measurement*, *23*(1),

676   R1–R38. https://doi.org/10.1088/0967-3334/23/1/201

677 Euler, M. J., Wiltshire, T. J., Niermeyer, M. A., & Butner, J. E. (2016). Working

678   memory performance inversely predicts spontaneous delta and theta-band

679   scaling relations. *Brain Research, 1637*, 22–33.

680   https://doi.org/10.1016/j.brainres.2016.02.008

681 Favela, L. H. (2020). Cognitive science as complexity science. *WIREs Cognitive*

682   *Science, 11*(4), e1525. https://doi.org/https://doi.org/10.1002/wcs.1525

683 Garcia, C. A. (2020). *nonlinearTseries: Nonlinear Time Series Analysis.* Retrieved

684   from https://CRAN.R-project.org/package=nonlinearTseries

685 Ge, E., & Leung, Y. (2013). Detection of crossover time scales in multifractal

686   detrended fluctuation analysis. *Journal of Geographical Systems, 15*(2), 115–147.

687   https://doi.org/10.1007/s10109-012-0169-9

688 Goldberger, A. L., Amaral, L. A. N., Hausdorff, J. M., Ivanov, P. C., Peng, C.-K., &

689   Stanley, H. E. (2002). Fractal dynamics in physiology: Alterations with disease

690   and aging. *Proceedings of the National Academy of Sciences, 99*(suppl 1),

691   2466–2472. https://doi.org/10.1073/pnas.012579499

692 Gulich, D., & Zunino, L. (2014). A criterion for the determination of optimal

693   scaling ranges in DFA and MF-DFA. *Physica A: Statistical Mechanics and Its*

694   *Applications, 397*, 17–30. https://doi.org/10.1016/j.physa.2013.11.029

695 Hardstone, R., Poil, S.-S., Schiavone, G., Jansen, R., Nikulin, V. V., Mansvelder, H.

696   D., & Linkenkaer-Hansen, K. (2012). Detrended Fluctuation Analysis: A

697   Scale-Free View on Neuronal Oscillations. *Frontiers in Physiology, 3*.

698   https://doi.org/10.3389/fphys.2012.00450

699 Hausdorff, J. M., Purdon, P. L., Peng, C. K., Ladin, Z., Wei, J. Y., & Goldberger,

700   A. L. (1996). Fractal dynamics of human gait: Stability of long-range

701   correlations in stride interval fluctuations. *Journal of Applied Physiology, 80*(5),

702   1448–1457. https://doi.org/10.1152/jappl.1996.80.5.1448

703 Ihlen, E. A. F. (2012). Introduction to Multifractal Detrended Fluctuation Analysis

704   in Matlab. *Frontiers in Physiology, 3.* https://doi.org/10.3389/fphys.2012.00141

Ihlen, E. A. F., & Vereijken, B. (2010). Interaction-dominant dynamics in human cognition: Beyond 1/f? fluctuation. *Journal of Experimental Psychology: General, 139*(3), 436–463. https://doi.org/10.1037/a0019098

Kantelhardt, J. W., Koscielny-Bunde, E., Rego, H. H. A., Havlin, S., & Bunde, A. (2001). Detecting long-range correlations with detrended fluctuation analysis. *Physica A: Statistical Mechanics and Its Applications, 295*(3), 441–454. https://doi.org/10.1016/S0378-4371(01)00144-3

Kantelhardt, J. W., Zschiegner, S. A., Koscielny-Bunde, E., Havlin, S., Bunde, A., & Stanley, H. E. (2002). Multifractal detrended fluctuation analysis of nonstationary time series. *Physica A: Statistical Mechanics and Its Applications, 316*(1), 87–114. https://doi.org/10.1016/S0378-4371(02)01383-3

Kantz, H., & Schreiber, T. (2003). *Nonlinear Time Series Analysis*. Retrieved from /core/books/nonlinear-time-series-analysis/519783E4E8A2C3DCD4641E42765309C7

Kello, C. T., Brown, G. D. A., Ferrer-i-Cancho, R., Holden, J. G., Linkenkaer-Hansen, K., Rhodes, T., & Orden, G. C. V. (2010). Scaling laws in cognitive sciences. *Trends in Cognitive Sciences, 14*(5), 223–232. https://doi.org/10.1016/j.tics.2010.02.005

Kelty-Stephen, D. G. (2017). Threading a multifractal social psychology through within-organism coordination to within-group interactions: A tale of coordination in three acts. *Chaos, Solitons & Fractals, 104*, 363–370. https://doi.org/10.1016/j.chaos.2017.08.037

Kelty-Stephen, D. G., Stirling, L. A., & Lipsitz, L. A. (2016). Multifractal temporal correlations in circle-tracing behaviors are associated with the executive function of rule-switching assessed by the Trail Making Test. *Psychological Assessment, 28*(2), 171–180. https://doi.org/10.1037/pas0000177

Kristoufek, L. (2013). Mixed-correlated ARFIMA processes for power-law

732   cross-correlations. *Physica A: Statistical Mechanics and Its Applications*,

733   *392*(24), 6484–6493. https://doi.org/10.1016/j.physa.2013.08.041

734   Kristoufek, L. (2015a). Detrended fluctuation analysis as a regression framework:

735   Estimating dependence at different scales. *Physical Review E*, *91*(2), 022802.

736   https://doi.org/10.1103/PhysRevE.91.022802

737   Kristoufek, L. (2015b). Detrended fluctuation analysis as a regression framework:

738   Estimating dependence at different scales. *Physical Review E*, *91*(2), 022802.

739   https://doi.org/10.1103/PhysRevE.91.022802

740   Laib, M., Golay, J., Telesca, L., & Kanevski, M. (2018). Multifractal analysis of the

741   time series of daily means of wind speed in complex regions. *Chaos, Solitons &*

742   *Fractals*, *109*, 118–127. https://doi.org/10.1016/j.chaos.2018.02.024

743   Legrand, P., & Véhel, J. L. (2003). Signal and image processing with FracLab.

744   *Thinking in Patterns: Fractals and Related Phenomena in Nature*, 321322.

745   Likens, A. D., Amazeen, P. G., West, S. G., & Gibbons, C. T. (2019a). Statistical

746   properties of Multiscale Regression Analysis: Simulation and application to

747   human postural control. *Physica A: Statistical Mechanics and Its Applications*,

748   *532*, 121580. https://doi.org/10.1016/j.physa.2019.121580

749   Likens, A. D., Amazeen, P. G., West, S. G., & Gibbons, C. T. (2019b). Statistical

750   properties of Multiscale Regression Analysis: Simulation and application to

751   human postural control. *Physica A: Statistical Mechanics and Its Applications*,

752   *532*, 121580. https://doi.org/10.1016/j.physa.2019.121580

753   Likens, A. D., Fine, J. M., Amazeen, E. L., & Amazeen, P. G. (2015). Experimental

754   control of scaling behavior: What is not fractal? *Experimental Brain Research*,

755   *233*(10), 2813–2821. https://doi.org/10.1007/s00221-015-4351-4

756   Likens, A. D., & Stergiou, N. (2020). *A tutorial on fractal analysis of human*

757   *movements* (N. Stergiou, Ed.). London, United Kingdom: Elsevier.

758   https://doi.org/10.1016/B978-0-12-813372-9.00010-5

Marmelat, V., & Meidinger, R. L. (2019). Fractal analysis of gait in people with parkinson's disease: Three minutes is not enough. *Gait & Posture*. https://doi.org/10.1016/j.gaitpost.2019.02.023

Moulder, R. G., Boker, S. M., Ramseyer, F., & Tschacher, W. (2018). Determining synchrony between behavioral time series: An application of surrogate data generation for establishing falsifiable null-hypotheses. *Psychological Methods*, *23*(4), 757–773. https://doi.org/10.1037/met0000172

Nagy, Z., Mukli, P., Herman, P., & Eke, A. (2017). Decomposing multifractal crossovers. *Frontiers in Physiology*, *8*. Retrieved from https://www.frontiersin.org/articles/10.3389/fphys.2017.00533

Peng, C.-K., Buldyrev, S. V., Havlin, S., Simons, M., Stanley, H. E., & Goldberger, A. L. (1994). Mosaic organization of DNA nucleotides. *Physical Review E*, *49*(2), 1685–1689. https://doi.org/10.1103/PhysRevE.49.1685

Perakakis, P., Taylor, M., Martinez-Nieto, E., Revithi, I., & Vila, J. (2009). Breathing frequency bias in fractal analysis of heart rate variability. *Biological Psychology*, *82*(1), 82–88. https://doi.org/10.1016/j.biopsycho.2009.06.004

Podobnik, B., & Stanley, H. E. (2008). Detrended Cross-Correlation Analysis: A New Method for Analyzing Two Nonstationary Time Series. *Physical Review Letters*, *100*(8), 084102. https://doi.org/10.1103/PhysRevLett.100.084102

Qian, X.-Y., Gu, G.-F., & Zhou, W.-X. (2011). Modified detrended fluctuation analysis based on empirical mode decomposition for the characterization of anti-persistent processes. *Physica A: Statistical Mechanics and Its Applications*, *390*(23), 4388–4395. https://doi.org/10.1016/j.physa.2011.07.008

Roume, C., Almurad, Z. M. H., Scotti, M., Ezzina, S., Blain, H., & Delignières, D. (2018). Windowed detrended cross-correlation analysis of synchronization processes. *Physica A: Statistical Mechanics and Its Applications*, *503*, 1131–1150. https://doi.org/10.1016/j.physa.2018.08.074

786 Santos, D. A., & Duarte, M. (2016). A public data set of human balance

787 evaluations. *PeerJ*, *4*, e2648. https://doi.org/10.7717/peerj.2648

788 Schaworonkow, N., & Voytek, B. (2021). Longitudinal changes in aperiodic and

789 periodic activity in electrophysiological recordings in the first seven months of

790 life. *Developmental Cognitive Neuroscience*, *47*, 100895.

791 https://doi.org/10.1016/j.dcn.2020.100895

792 Schreiber, T., & Schmitz, A. (1996). Improved surrogate data for nonlinearity tests.

793 *Physical Review Letters*, *77*(4), 635–638.

794 https://doi.org/10.1103/PhysRevLett.77.635

795 Shen, C. (2015). Analysis of detrended time-lagged cross-correlation between two

796 nonstationary time series. *Physics Letters A*, *379*(7), 680–687.

797 https://doi.org/10.1016/j.physleta.2014.12.036

798 Snow, E. L., Likens, A. D., Allen, L. K., & McNamara, D. S. (2016). Taking

799 Control: Stealth Assessment of Deterministic Behaviors Within a Game-Based

800 System. *International Journal of Artificial Intelligence in Education*, *26*(4),

801 1011–1032. https://doi.org/10.1007/s40593-015-0085-5

802 Stephen, D. G., Boncoddo, R. A., Magnuson, J. S., & Dixon, J. A. (2009). The

803 dynamics of insight: Mathematical discovery as a phase transition. *Memory &*

804 *Cognition*, *37*(8), 1132–1149. https://doi.org/10.3758/MC.37.8.1132

805 Team, R. C. (2018). *R: A language and Environment for Statistical Computing.*

806 Vienna, Austria.

807 Van Orden, G. C., Holden, J. G., & Turvey, M. T. (2003). Self-organization of

808 cognitive performance. *Journal of Experimental Psychology: General*, *132*(3),

809 331–350. https://doi.org/10.1037/0096-3445.132.3.331

810 Wiltshire, T. J., Steffensen, S. V., & Fiore, S. M. (2019). Multiscale movement

811 coordination dynamics in collaborative team problem solving. *Applied*

812 *Ergonomics*, *79*, 143–151. https://doi.org/10.1016/j.apergo.2018.07.007

Xu, L., Ivanov, P. Ch., Hu, K., Chen, Z., Carbone, A., & Stanley, H. E. (2005). Quantifying signals with power-law correlations: A comparative study of detrended fluctuation analysis and detrended moving average techniques. *Physical Review E*, *71*(5), 051101. https://doi.org/10.1103/PhysRevE.71.051101

Zebende, G. F. (2011). DCCA cross-correlation coefficient: Quantifying level of cross-correlation. *Physica A: Statistical Mechanics and Its Applications*, *390*(4), 614–618. https://doi.org/10.1016/j.physa.2010.10.022

Table 1

Table 1. Overview of core package functions, objectives, and output

Function	Objective	Output
`dfa()`	Estimate long-range correlation in a time series	Object containing the overall α estimate and, if desired the `logScales` and `logRMS`
`mfdfa()`	Estimate the magnitude and range of long-range correlations in a time series	Object containing the log scales used for the analysis, the log fluctuation function for each scale and q, the various q-order exponents, Hq, Tau, h, and Dh. The base of *log* depends on scale construction and user input
`dcca()`	Estimates of scale-specific correlation between two time-series	Object containing the scales used for the analysis and the ρ 'rho' values for each scale
`mra()`	Estimates the scale specific regression coefficients for a predictor time series on and outcome time series	Object containing the scales and scale specific β estimates, R^2, and t statistics
`fgn_sim()`	Simulate univariate fractional Gaussian noise	Returns a vector of length `N` according to the specified `H` Hurst exponent

Function	Objective	Output
`mBm_mGn()`	Simulate univariate multi-fractional Brownian motion and Gaussian noise	Returns two vectors of length `N` according to the specified H_t series
`mc_ARFIMA()`	Simulate various types of bivariate correlated noise processes.	Returns two vectors of length `N` according to the specified noise `process` and parameters
`iaaft()`	Generate surrogate series using the iterative amplitude adjusted Fourier transform	Returns a vector of same length as input time series

Table 2

Results from piece-wise regression analysis

	Estimate	SE	t	95% CI l	95% CI u
Slope 1	1.36	0.03	40.66	1.30	0.40
Slope 2	0.43	0.01	31.25	1.43	0.45

Table 3

Table 3. Overview of development plan for `fractalRegression` package

Function	Next Release	Future Release
DLCCA	X	
MLRA	X	
Chabra-Jensen's Direct Estimation of Multifractal Spectra	X	
Wavelet Based Fractal Analyses		X
Multifractal Cross-Correlation Methods		X
Advanced Detrending Methods		X
Bayesian Estimation of Hurst Exponent		X
Time Lag Optimization Function		X